Hydration Energies of Zinc(II): Threshold Collision-Induced Dissociation Experiments and Theoretical Studies

Theresa E. Cooper, D. R. Carl, and P. B. Armentrout*

Department of Chemistry, University of Utah, 315 S. 1400 E. Rm 2020, Salt Lake City, Utah 84112

Received: July 2, 2009; Revised Manuscript Received: September 8, 2009

The first experimentally determined sequential bond dissociation energies of $Zn^{2+}(H_2O)_n$ complexes, where $n = 6-10$, are measured using threshold collision-induced dissociation in a guided ion beam tandem mass spectrometer coupled with an electrospray ionization source. Kinetic energy dependent cross sections are obtained and analyzed to yield 0 K threshold measurements for the loss of one and two water ligands after accounting for multiple collisions, kinetic shifts, and energy distributions. The threshold measurements are then converted from 0 to 298 K values to give the hydration energies for sequentially losing one water from each parent complex. Theoretical geometry optimizations and single-point energy calculations are performed using several levels of theory for comparison to experiment. Although different levels of theory disagree on the ground-state conformation of most complexes examined here leading to potential ambiguities in the final thermochemical values, calculations at the MP2(full) level provide the best agreement with experiment. On this basis, the present experiments are most consistent with the inner solvent shell of Zn^{2+} being five waters, except for $Zn^{2+}(H_2O)_6$ where all waters bind directly to the metal ion. The charge separation process, $Zn^{2+}(H_2O)_n \rightarrow ZnOH^+(H_2O)_m + H^+(H_2O)_{n-m-1}$, which is in competition with the loss of water from the parent complex, is also observed for $n = 6-8$. These processes are analyzed in detail in the following paper.

Introduction

Zinc solvation and coordination behavior is of paramount importance in the fields of biochemistry and bioinorganic chemistry as the zinc ion is required for the activation of certain proteins and metalloenzymes.[1−3] Thus, zinc is biologically important and not toxic. In addition, zinc metal consumption ranks fourth in the world among all metals.[4] The most common uses are to galvanize steel, as a component in brass, and as an additive in rubbers and paints.[4] Such high usage implies large discharges to the environment, such that zinc is quickly infiltrating aqueous systems, thereby making its way into the food chain, drinking water, and eventually the atmosphere.

Zinc coordination behavior has previously been studied using a variety of experimental methods including Raman spectroscopy on aqueous $Zn^{2+}(ClO_4)_2$,[5] ion equilibria using a variety of ligands (but not water),[6−8] collision-induced dissociation (CID) mass spectrometry of the hydrated ion,[9,10] and X-ray absorption fine structure studies of the ion in aqueous media.[11] Despite this activity, experimental thermochemistry for the hydration of zinc cations is presently unknown. Because of the lack of experimental bond energies, a host of theoretical work has been performed utilizing a variety of quantum chemical and Monte Carlo calculations including density functional theory (DFT), Hartree−Fock (HF), and molecular dynamics simulations.[5−9,11−18]

Neither experiment nor theory has yet established definitively the number of waters in the inner solvent shell surrounding the zinc cation in $Zn^{2+}(H_2O)_n$ complexes. X-ray, Raman, and near-IR spectroscopy report a coordination number of six forming an octahedral inner shell, which until recently has been the commonly accepted configuration.[3,5,11,19] Using quantum chemical calculations, several studies found the differences in energies between inner solvent shells of four, five, and six water molecules to be very small.[14,15,18] Indeed, the lowest energy complex switches between an inner shell of four or six depending on the level of theory used. An inner shell of six is favored by MP2 calculations, whereas B3LYP theory has a slight preference for an inner shell of four.[14−16,18] Pavlov et al.[18] theorized that calculations of larger clusters ($n > 12$) are needed to accurately represent the dilute solutions explored by X-ray scattering, Raman, and near-IR experiments. However, such conclusions are clearly influenced by the basis set size, as demonstrated by Peschke et al.[8] for the Zn^{2+} ion interacting with acetone ligands. They found large energy differences when geometries were calculated using B3LYP/6-311++G(d,p) compared to the values given in the B3LYP/LANL2DZ calculations reported by Pavlov et al.[18]

To address the lack of thermochemical information on the hydration energies of the zinc cation, the present study examines the dissociation behavior of $Zn^{2+}(H_2O)_n$ complexes where $n = 7-10$. In all cases, the dominant process observed is reaction 1 followed by sequential loss of additional water molecules.

$$Zn^{2+}(H_2O)_n \rightarrow Zn^{2+}(H_2O)_{n-1} + H_2O \qquad (1)$$

Analysis of the kinetic energy dependence of these reactions provides the first experimental determinations of the hydration energies of zinc cation−water complexes. These values are compared to previous and present theoretical calculations, which also examine the issue of the size of the inner solvent shell.

In addition, particular sized complexes are found to undergo a charge separation process, reaction 2, which is discussed in detail in the following paper.[20]

* To whom correspondence should be addressed.

10.1021/jp906235y CCC: $40.75
Published on Web 11/11/2009

$$Zn^{2+}(H_2O)_n \rightarrow ZnOH^+(H_2O)_m + H^+(H_2O)_{n-m-1} \quad (2)$$

One result from the analysis in that work that is important here is that competition between reactions 1 and 2 does influence the experimental thresholds for reaction 1 with $n \leq 7$ and this effect is included in the thermochemistry reported here. Finally, we note that because the threshold for charge separation is below the threshold for water loss for $n = 7$, electrospray ionization (ESI) sources are generally limited to producing $Zn^{2+}(H_2O)_7$ and larger complexes.

Theoretical and Experimental Section

Computational Details. Because there is a debate in the literature regarding the calculated ground state of the $Zn^{2+}(H_2O)_n$ complexes, a simulated annealing procedure using the AMBER (Version 8) program[21] was used to generate all possible low-lying isomers. Annealing procedures were followed three independent times for inner hydration shells of four, five, or six water ligands. To constrain the inner shell to these sizes, an energetic barrier was used to prevent waters from moving too far from the metal ion, and applied to the second-shell waters (when applicable) preventing these ligands from entering into the first shell. Each isomer was then optimized using a low level of ab initio theory, HF/3-21G.[22,23] Using the Gaussian03 package,[24] further geometry optimizations were performed on the lowest lying isomers generated from the annealing process (about 50 structures for the larger complexes). These structures were first optimized at the B3LYP/6-31G(d) level[25−27] in a "loose" geometry optimization, which utilizes a large step size (0.01 au) and rms force constant (0.0017) to give a rapid geometry convergence. The lowest energy structures (about 25) were further optimized with a larger basis set, B3LYP/6-311+G(d,p). This level of theory was used for the final geometry optimizations as well as providing vibrational frequencies and rotational constants.

These calculated frequencies and rotational constants were used in the RRKM thermochemical analysis discussed below, as well as for zero point energy (ZPE) conversions of theoretical bond dissociation energies to 0 K thermochemical values. The vibrational frequencies were each scaled by 0.989[28] before being used in these analyses. Using these geometries, single point energy (SPE) calculations were performed using the B3LYP, B3P86,[29] and MP2(full)[30] levels of theory with a 6-311+G(2d,2p) basis set. As will be seen below, conflicting results are provided by these two DFT levels versus the MP2(full) calculations. To explore which set of results is more likely to be accurate, a third DFT calculation was performed using the M06[31,32] functional, which was developed specifically for noncovalent interactions found in ion solvation and hydration. Accordingly, additional SPE energies were calculated using the M06 level with a 6-311+G(2d,2p) basis set. Diffuse functions were used in the geometry optimization, frequency calculation, and SPE calculations because of their importance for describing the hydrogen bonding of the zinc water clusters. Previous works have discussed this importance in both zinc hydration and solvation.[8,18] Basis set superposition errors (BSSE) were also calculated for dissociation of the lowest energy structures at each level of theory in the full counterpoise (cp) limit.[33,34] The BSSE corrections found for all three DFT calculations were relatively small, ≤5 kJ/mol, and slightly larger for the MP2(full) level, 8−10 kJ/mol depending on the size of the complex. For simplicity purposes, when these four levels of theory are discussed the B3LYP and B3P86 levels will be abbreviated together as "Bx" and the M06 and MP2(full) will be abbreviated together as "Mx". In addition to the Bx and Mx results, we also performed BHandHLYP[35]/6-311++G(2d,2p)//BHandHLYP/6-311++G(d,p) calculations (which were shown in a previous study[36] to be able to describe hydrogen bonding in amino acids as well as or better than computationally more expensive methods) for the lowest energy complexes of the four, five, and six water inner shells of $Zn^{2+}(H_2O)_6$. (Identical geometries were obtained using the 6-311+G(d,p) basis set.) BHandHLYP results show that the six water inner shell is the lowest energy structure, but the other two complexes are ∼2 kJ/mol above the ground state, similar to the MP2(full) level discussed in more detail below.

In addition to the B3LYP and BHandHLYP geometry optimizations performed, we also calculated MP2(full)/6-311+G(d,p) geometries for $Zn^{2+}(H_2O)_n$ for $n = 5-9$, M06/6-311+G(d,p) geometries for $n = 6-10$, and B3LYP/6-311++G(d,p) geometries for $n = 6$ and 9, along with their corresponding SPEs at the same three levels of theory used above. No discernible differences in the geometries and energetics were found using these more expensive approaches. Hence, results from the B3LYP/6-311+G(d,p) geometry optimizations are used exclusively in the discussion below.

Experimental Procedures. Hydrated zinc dications are generated using an ESI source,[37] comprising a stainless steel electrospray needle, a heated capillary, an 88 plate ion funnel, and a hexapole ion guide where the ions undergo sufficient thermalizing collisions to bring them to a Maxwell−Boltzmann distribution at ambient temperatures. $Zn^{2+}(H_2O)_n$ clusters are formed by passing a dilute solution of $Zn(NO_3)_2$, 10^{-4} M in water, through the electrospray needle at a low flow rate of 0.02−0.10 mL/h with a high voltage applied to the needle, typically 2.0−2.2 kV. The capillary following the spray is heated to 80 °C to promote desolvation of large droplets and has a small applied potential, typically <15 V. The ion funnel[38] collects the ions emitted from the capillary thereby increasing signal intensity.[39,40] The ions are pulled through the funnel by a gentle dc gradient, typically 5−8 V, and undergo multiple collisions with the ambient gas. The radio frequency (rf) hexapole ion guide/collision cell traps the ions in the radial direction using an rf amplitude typically set at 250 V peak to peak. Here, the ions undergo $>10^4$ collisions with the ambient gas as they drift through the hexapole, such that the ions emerging are thermalized, as shown previously.[37,41−43] Compared to previous settings used in our lab, the source conditions needed to generate $Zn^{2+}(H_2O)_n$ complexes are unusually gentle because of the charge separation process 2. If larger voltage drops between components of the source are used, copious amounts of $ZnOH^+(H_2O)_n$ and $H^+(H_2O)_m$ are produced, thereby limiting the intensity of the desired zinc water clusters. The dc fin electrodes, an in source fragmentation technique described in more detail elsewhere,[44] were used to increase the amount of the $Zn^{2+}(H_2O)_7$ complex produced by our ESI. Increasing the voltage on the fins tends to form smaller metal hydrate complexes as described by Carl et al.;[44] however, for the case of zinc hydration increasing the fin voltage past the intensity peak for the $n = 7$ complex generated charge separation products and no complexes smaller than $n = 7$ were observed from our source.

Kinetic energy dependent cross sections for collision-induced dissociation of the $Zn^{2+}(H_2O)_n$ complexes are measured using our guided ion beam tandem mass spectrometer described in detail elsewhere.[45,46] The ions generated as described above are

focused into a magnetic momentum analyzer, which selects the desired reactant zinc water complex. The reactant is decelerated to a known potential relative to the ion source, V_{Lab}, and focused into an rf octopole ion guide where the ion is trapped radially.[47] A collision gas cell surrounds part of the octopole and contains xenon, which is introduced to the collision cell at pressures varying between 0.05 and 0.20 mTorr. Xenon makes an excellent choice for inducing dissociation as it is heavy, monatomic, polarizable, and chemically unreactive.[48,49] After collision, reactant and product ions drift to the end of the octopole guide, where they are focused into a quadrupole mass filter for mass analysis and then detected utilizing a Daly detector.[50]

As described elsewhere,[45] ion intensities are converted to absolute cross sections with an uncertainty of ±20%. In addition, the laboratory potential of the ions, V_{Lab}, is converted to the relative kinetic energy in the center-of-mass (CM) frame using $E_{CM} = 2\ V_{Lab}m/(m + M)$, where m is the mass of the neutral collision gas, M is the mass of the ionic reactant, and the factor of 2 accounts for the charge on the reactant complexes. The absolute energy zero and kinetic energy distribution of the reactant ions are determined using a retarding potential technique.[45] The derivative of the normalized ion intensities is fit to a Gaussian distribution, with a full width at half-maximum (fwhm) in V_{Lab} that ranges in these experiments from 0.08 to 0.15 eV. The absolute uncertainty in V_{Lab} is 0.05 eV. For the remainder of this paper, all energies are reported in the CM frame.

Threshold Modeling. In order to extract accurate thermochemical results from analysis of the kinetic energy dependent cross sections, several factors must be considered. Experiments were performed at three different pressures of Xe (typically about 0.05, 0.10, and 0.20 mTorr) and the resulting cross sections extrapolated to a zero pressure cross section to ensure single-collision conditions.[51,52] This rigorously removes effects arising from multiple collisions, which are particularly significant in the present system for higher order water losses and the charge separation channels. Using this zero pressure cross section, the loss of a single water molecule from a reactant $Zn^{2+}(H_2O)_n$ complex is modeled using eq 3.

$$\sigma(E) = \sigma_0 \sum g_i (E + E_i - E_0)^N / E \qquad (3)$$

In this modified line-of-centers expression, σ_0 is an energy independent scaling factor, E is the relative translational energy of the reactants, E_0 is the reaction threshold at 0 K, and N is an adjustable fitting parameter that characterizes the energy deposition during collision.[46] The summation is over the rovibrational states of the reactants having excitation energies E_i and populations g_i, where $\sum g_i = 1$. The number of rovibrational states is directly counted using the Beyer−Swinehart Stein−Rabinovitch algorithm,[53−56] and a Maxwell−Boltzmann distribution is used to describe the populations g_i. Before comparison with the data, the model is also convoluted over the kinetic energy distributions of the reactants.[45]

The complexes examined in the present study are sufficiently large that their dissociation lifetime near the dissociation threshold is comparable to the experimental time of flight, $\tau \approx 5 \times 10^{-4}$ s in this apparatus. This behavior can give rise to a kinetic shift that can be estimated by incorporating Rice−Ramsperger−Kassel−Marcus (RRKM) theory[56,57] into eq 3, as discussed in detail elsewhere.[58−60] In addition, theoretical results discussed in the section below show that a distribution of different reactant and product isomers are possible. To account for the competition between these multiple dissociation pathways, which in this case yield product ions having the same mass, statistical theory can be used for each individual reaction channel j, as discussed elsewhere.[61] With both of these changes, eq 3 is modified to eq 4

$$\sigma_j(E) = (N\sigma_{0,j}/E) \sum g_i \int_{E_{0,j}-E_i}^{E} [k_j(E^*)/k_{tot}(E^*)] P_{D1}(E - \varepsilon)^{N-1}\, d(\varepsilon) \qquad (4)$$

where ε is the energy transferred into the reactant ion by the collision such that the energy available for dissociation is $E^* = \varepsilon + E_i$. $P_{D1} = 1 - \exp[-k_{tot}(E^*)\tau]$ is the probability of dissociation of the energized molecule, EM. Should the unimolecular rate constant be sufficiently fast for complete dissociation, eq 4 reduces to eq 3 for a single channel. The RRKM unimolecular rate constants for dissociation are given by eq 5

$$k_{tot}(E^*) = \sum k_j(E^*) = \sum s_j N^{\dagger}_{vr,j}(E^* - E_{0,j})/h\rho_{vr}(E^*) \qquad (5)$$

where s_j is the reaction degeneracy for channel j given by the ratio of the rotational symmetry numbers (reactant/products),[56] $N^{\dagger}_{vr,j}$ is the number of rovibrational states of the transition state (TS) for channel j at an energy $E^* - E_{0,j}$ above the reaction barrier, and $\rho_{vr}(E^*)$ is the density of states for the rovibrational levels of the EM. The rotational constants and vibrational frequencies of the EM and TSs are taken from quantum chemical calculations (detailed above). For water loss channels, the transition state is loose as the bond cleavage is heterolytic with all the charge remaining on the complex containing the zinc ion.[62] The TS for water loss is treated at the phase space limit (PSL) in which the transitional modes are treated as rotors.[60] In this limit, the TS is product-like such that its molecular parameters are taken from quantum chemical calculations of the products.

Because the charge separation process 2 prevents clusters smaller than $Zn^{2+}(H_2O)_7$ from being formed in our source, CID studies were limited to complexes of $n = 7-10$. In order to obtain thermochemical information on smaller complexes, thresholds for sequential dissociation were modeled in conjunction with modeling the single water loss channel, reaction 1. A statistical approach to modeling sequential dissociation has recently been developed and proven to provide accurate thresholds for singly charged systems.[63] This model makes statistical assumptions regarding the energy deposition in the products of the initial CID reaction. Ultimately, this model assigns a probability for further dissociation of the product of reaction 1

$$P_{D2} = 1 - \exp[-k_2(E_2^*)\tau] \qquad (6)$$

where E_2^* is the internal energy of the product ion undergoing sequential dissociation. This energy is determined by energy conservation, i.e., $E_2^* = E^* - E_0 - T_1 - E_L$, where T_1 is the translational energy of the primary products and E_L is the internal energy of the neutral product. Statistical assumptions are used to assign the distributions of each of these quantities, thereby allowing calculation of the secondary dissociation rate constant, k_2. Because of the complexity of the sequential dissociation model, its use is presently limited to single primary

TABLE 1: B3LYP/6-311+G(d,p) Geometry Optimized Structures for Ground State $Zn^{2+}(H_2O)_{1-4}$[a]

complex	symmetry	r(ZnO) (Å)	∠OZnO (deg)	∠ZnOH (deg)	r(OH) (Å)	∠HOH (deg)
H_2O	C_{2v}				0.962 (2)	105.1
$Zn^{2+}(H_2O)$	C_{2v}	1.881		125.3 (2)	0.984 (2)	109.5
$Zn^{2+}(H_2O)_2$	D_{2d}	1.876 (2)	180.0	125.6 (4)	0.979 (4)	108.8 (2)
$Zn^{2+}(H_2O)_3$	C_2	1.944 (2)	120.0 (3)	125.3 (2)	0.974 (4)	107.9 (2)
		1.953		126.8 (2)	0.979 (2)	107.2
				126.4 (2)		
$Zn^{2+}(H_2O)_4$	S_4	2.002 (4)	105.1 (2)	126.0 (4)	0.970 (8)	107.6 (4)
			111.7 (4)	126.3 (4)		

[a] Values in parentheses indicate degeneracies.

TABLE 2: Relative Calculated Enthalpy (ΔH_0) and Free Energies (ΔG_{298})[a] (kJ/mol) of $Zn^{2+}(H_2O)_x(H_2O)_y$ Where x is the Number of Waters in the Inner Solvent Shell and y is the Number of Waters in the Second Shell[b]

		present work				literature			
complex (x,y)		B3LYP// B3LYP	B3P86// B3LYP	M06// B3LYP	MP2(full)// B3LYP	B3LYP// B3LYP[c]	B3LYP// B3LYP[d]	MP2(FC)// RHF[e]	MP2// HF[f]
$Zn^{2+}(H_2O)_5$	(4,1)_AA	0.0 (2.6)	0.0 (2.9)	6.5 (8.2)	3.3 (4.3)	0.0	0.0	2.5	3.8 (0.0)
	(4,1)_A	1.1 (0.0)	0.8 (0.0)	14.9 (12.9)	8.4 (5.7)				
	(5,0)	4.2 (5.8)	4.6 (6.4)	0.0 (0.6)	0.0 (0.0)	4.2	1.7	0.0	0.0 (0.4)
	(5,0)_switch	5.8 (5.4)	6.0 (5.8)	1.4 (0.0)	2.4 (0.3)				
$Zn^{2+}(H_2O)_6$	(4,2)_2AA	0.0 (0.0)	0.0 (0.0)	13.1 (12.8)	3.8 (7.5)	0.0	0.0	0.0	18.8 (12.6)
	(5,1)_A_aA_b	8.2 (0.3)	8.6 (0.6)	12.2 (4.1)	4.2 (0.0)	20.5	4.2	1.5	16.7 (3.8)
	(5,1)_A_a	17.1 (3.1)	17.4 (3.3)	26.6 (12.3)	16.9 (6.6)	15.5			26.4 (11.3)
	(6,0)	13.7 (14.0)	14.6 (14.8)	0.0 (0.0)	0.0 (3.9)	14.2	4.6	0.6	0.0 (0.0)
$Zn^{2+}(H_2O)_7$	(4,3)_3D,DD_2AA,A	0.0 (6.5)	0.0 (6.5)	14.9 (9.6)	10.8 (5.5)				
	(4,3)_2D,DD_AA,2A	4.1 (0.0)	4.1 (0.0)	23.6 (7.7)	18.0 (2.1)				
	(4,3)_2D,2DD_3AA	10.1 (23.0)	10.2 (23.0)	17.9 (18.9)	18.1 (19.1)				
	(5,2)_4D_2A_bA_b	0.2 (12.0)	0.1 (12.0)	0.0 (0.0)	0.0 (0.0)		0.0		
	(6,1)_AA	18.4 (31.3)	18.7 (31.6)	3.2 (4.3)	8.7 (9.7)		20.1		
$Zn^{2+}(H_2O)_8$	(4,4)_2D,2DD_2AA,2A	1.8 (0.0)	2.4 (0.1)	21.4 (12.5)	14.9 (6.1)				
	(5,3)_3AA	0.0 (7.1)	0.0 (6.6)	0.0 (0.0)	0.0 (0.0)				
	(6,2)_2D,DD_2AA	16.8 (23.5)	17.7 (23.9)	2.1 (1.7)	6.7 (6.3)				
	(6,2)_4D_2AA	17.7 (25.0)	17.8 (24.6)	2.0 (2.2)	7.3 (7.5)				
$Zn^{2+}(H_2O)_9$	(4,5)_D,3DD_2AA,3A	5.8 (0.0)	6.3 (0.0)	30.7 (14.6)	22.1 (6.0)				
	(5,4)_4A_bA_b	0.0 (10.3)	0.0 (9.8)	0.0 (0.0)	0.0 (0.0)				
	(6,3)_6D_3AA	13.5 (27.9)	13.1 (26.9)	2.8 (7.0)	3.9 (8.0)				
	(6,3)_4D,DD_3AA	16.9 (26.0)	16.7 (25.3)	4.5 (3.3)	7.2 (6.0)				
$Zn^{2+}(H_2O)_{10}$	(4,6)_2AA,4A	3.5 (0.0)	4.4 (0.0)	26.9 (16.3)	18.6 (8.0)				
	(5,5)_4A_bA_b,A_a	0.0 (7.1)	0.0 (6.2)	0.0 (0.0)	0.0 (0.0)				
	(6,4)_4D,2DD_4AA	18.1 (35.5)	16.9 (33.5)	0.0 (10.3)	5.5 (15.9)				

[a] ΔG_{298} values given in parentheses. [b] Values are single-point energies calculated at the level shown using a 6-311+G(2d,2p) basis set with geometries calculated at the B3LYP/6-311+G(d,p) level. Zero point energy corrections are included. [c] Values reported by Pavlov et al.[18] using a B3LYP/6-311+G(2d,2p)//B3LYP/LANL2DZ level of theory. [d] Values reported by Hartmann et al.[15] using a B3LYP/SHA1//B3LYP/SHA3 level of theory. [e] Values reported by Bock et al.[14] using a MP2(FC)/HUZSP*//RHF/HUZSP* level of theory. [f] Values reported by Lee et al.[16] using a MP2/TZ2P//HF/TZ2P level of theory.

product channels such that no designation of the individual reaction channel j is included in eq 6.

Analysis of the data involves using eqs 3 or 4 to reproduce the data over extended energy and magnitude ranges, using a least-squares criterion for optimizing the fitting parameters, $\sigma_{0,j}$, $E_{0,j}$, and N. The uncertainties in these parameters include variations associated with modeling several independent experimental cross sections, scaling the theoretical vibrational frequencies by ±10%, varying the N value by ±0.1, scaling the experimental time-of-flight up and down by a factor of 2, and the uncertainty in the absolute energy scale.

Results and Discussion

Theoretical Geometries of Zinc Water Clusters. As described above, geometry optimizations and frequency calculations were performed at the B3LYP/6-311+G(d,p) level of theory. Although experimental data for the $Zn^{2+}(H_2O)_n$ complexes where $n = 1-5$ are not accessible at this time, for completeness, these structures were also optimized and SPEs calculated at the same theoretical levels designated above.

In agreement with previous theoretical results performed on these smaller complexes,[5,8,15−18] all waters bind directly to the zinc metal ion for $n = 1-4$. In all four species, the water ligands are distributed to maximize the distance between ligands, such that the oxygen atoms are located in linear, distorted trigonal planar, and near-tetrahedral geometries for $n = 2-4$, respectively. Key structural parameters for these smaller complexes are provided in Table 1.

For larger cluster sizes, $n \geq 5$, there is a debate as to the number of waters in the inner shell of the ground-state structure. Both Hartmann et al. and Lee et al. examined the possibility of having an inner shell of 3 water ligands at the $n = 4$ and 5 complexes and both studies found that these structures were very high in energy.[15,16] In the present work, several isomers of the $n = 5-10$ clusters (excluding the 3 water inner shell) were explored theoretically, with energy differences for low-energy isomers presented in Table 2. The lowest energy structures having inner solvent shells of 4, 5, and 6 water ligands are shown in Figures 1−3 for the $n = 6-8$ complexes, whereas those for $n = 9$ and 10 are shown in Figures S1 and S2 of the Supporting Information. In most cases, when a second-shell water ligand forms two hydrogen bonds to the inner shell (indicated by an AA designation), the structure is lower in energy than if there is only one hydrogen bond to the inner

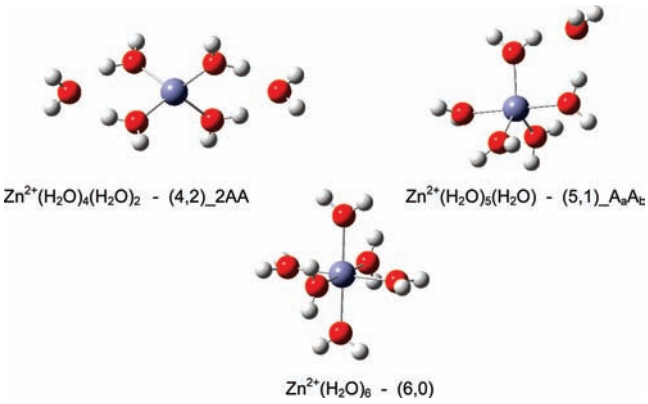

Figure 1. Low-energy isomers of $Zn^{2+}(H_2O)_6$ calculated at the B3LYP/6-311+G(d,p) level of theory.

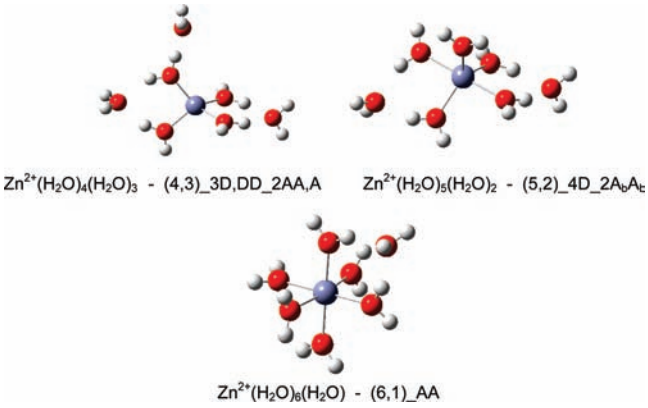

Figure 2. Low-energy isomers of $Zn^{2+}(H_2O)_7$ calculated at the B3LYP/6-311+G(d,p) level of theory.

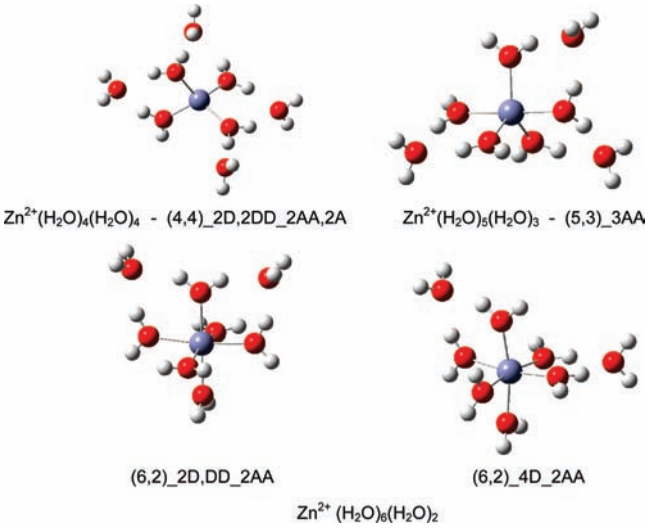

Figure 3. Low-energy isomers of $Zn^{2+}(H_2O)_8$ calculated at the B3LYP/6-311+G(d,p) level of theory.

shell (indicated by A). A number of additional higher energy isomers were also calculated for all inner-shell sizes of the $n = 6-10$ complexes. Because of the large number of isomers investigated, their geometries and relative energetics are discussed in more detail in the Supporting Information. (Table S1 of the Supporting Information lists relative energies for all isomers with key geometric parameters of all larger complexes provided in Table S2. Figure S3 shows the additional structures found.)

For $n = 5$, the present results find that the $Zn^{2+}(H_2O)_4(H_2O)_1$ or (4,1)_AA structure has a distorted tetrahedral inner solvent shell with the fifth water forming two hydrogen bonds to the inner shell (Figure S3a in Supporting Information). The nomenclature used here for these complexes specifies the number of inner-shell waters x and second-shell water ligands y by (x,y) augmented with the designation of the hydrogen bonding motif of the complex. The (4,1)_AA structure is slightly more stable at the Bx levels (B3LYP and B3P86) than the $Zn^{2+}(H_2O)_5$ or (5,0) structure with all five waters in the inner solvent shell forming a square pyramidal shape (Figure S3b) but Mx results (M06 and MP2(full)) find the opposite result (Table 2). The Bx results are in agreement with earlier DFT theoretical work performed on this size complex,[15,18] as are the MP2 results with analogous earlier calculations.[14,16] Alternate isomers include the (4,1)_A structure, which has the second-shell water singly hydrogen bonded to the inner shell and lies 1−15 kJ/mol higher than (4,1)_AA. Because the torsional motion of the outer water molecule is now much looser (nearly a free rotor), this structure has a lower 298 K free energy than (4,1)_AA at the Bx levels. Compared to the (5,0) structure, (5,0)_switch decreases the ∠OZnO bond angle of the two waters whose hydrogen atoms are pointing vertical to the base of the square pyramid, whereas ∠OZnO increases for the waters whose hydrogens are in the plane of the base (Figure S3b).

For $n = 6$, there are now three options for the size of the inner shell with (4,2), (5,1), and (6,0) configurations, where the latter has all six water ligands in the inner solvent shell in a pseudo-octahedral geometry. These optimized structures are shown in Figure 1 and are comparable to geometries in previous reports.[14−18] Bock et al. performed geometry optimizations and SPE calculations using a MP2(FC)/HUZSP*//RHF/HUZSP* level and found that the energy difference between (4,2)_2AA, (5,1)_AA, and (6,0) was less than 2 kJ/mol (Table 2).[14] In contrast, Lee et al. found a larger energetic difference favoring the (6,0) structure by almost 17 kJ/mol over the (4,2)_2AA and (5,1)_AA structure using MP2/TZ2P//HF/TZ2P calculations.[16] As for the $n = 5$ complex, B3LYP results provide a much different ordering. Pavlov et al. found a flexible coordination calculating the preference for (4,2)_2AA to be about 14−21 kJ/mol whereas the (5,1)_AA and (6,0) differ from each other by about 1 kJ/mol using a B3LYP/6-311+G(2d,2p)//B3LYP/LANL2DZ level of theory.[18] Hartmann et al. used a B3LYP/SHA3//B3LYP/SHA1 level of theory and found a preference toward the (4,2)_2AA complex by 4−5 kJ/mol over (5,1)_AA and (6,0).[15] Pavlov et al. and Lee et al. also included an alternative (5,1)_A geometry, which was found to be about 5 kJ/mol lower in energy than (5,1)_AA at the B3LYP level[18] but about 10 kJ/mol higher than (5,1)_AA at the MP2 level.[16]

As for these previous results, we find energy differences among the three possible structures of the $n = 6$ complex calculated here to be relatively small, <14 kJ/mol, with the ground state changing from (4,2)_2AA for Bx to (6,0) for Mx calculations (Table 2). In the lowest energy (4,2)_2AA isomer, both second solvent shell water molecules bind to the inner solvent shell through two hydrogen bonds (Figure 1). The (5,1)_A_aA_b structure binds the outer-shell water molecule to the apex water and one water in the base, abbreviated with the "a" and "b" subscripts, respectively. This arrangement necessitates rotation of one of the base water molecules, which disrupts some of the hydrogen bonding found in the (5,0) and (5,0)_switch structures. The (5,1)_A_a isomer has the sixth water singly hydrogen bound to the apex water of the square pyramid inner shell, such that it lies 9−14 kJ/mol above (5,1)_A_aA_b at 0 K, in contrast to the results of Pavlov et al. At 298 K, this excitation energy drops to 3−8 kJ/mol and the MP2(full) GS becomes

the (5,1)_A_aA_b complex, whereas (6,0) becomes the M06 ground state (Table 2). The (4,2)_2AA remains the GS for the Bx calculations at 298 K.

Larger complexes, $n = 7-10$, were optimized using the same basic inner-shell shapes. As many of these complexes have similar hydrogen bonding in the second solvation shell, our nomenclature includes terms "D" or "DD" to describe an inner-shell water that donates to a second-shell water with one or two hydrogen bonds, respectively. For the $n = 7$ complex, the 4- and 5-coordinate zinc ion structures are isoenergetic with each other at the two Bx levels of theory, whereas Mx calculations favor the 5-coordinate inner shell. These structures are shown in Figure 2. In the (4,3)_3D,DD_2AA,A complex, the seventh water is added to the (4,2)_2AA complex such that it forms only one hydrogen bond to the inner shell, which is much weaker than the two hydrogen bonds formed for the second-shell ligands in the (4,2)_2AA and (5,2)_4D_2A_bA_b complexes, as discussed further below. The (4,3) complex forms three higher energy isomers (Figure S3e). Among these, the (4,3)_2D,DD_AA,2A has two singly hydrogen-bound waters in the outer shell, where one of these is bound to an inner-shell water that also binds the bridging second-shell water. Although this complex is 4−9 kJ/mol higher in energy than (4,3)_3D,DD_2AA,A at 0 K, it has a lower free energy at 298 K by 2−7 kJ/mol. Interestingly, the (4,3)_2D,2DD_3AA isomer is highest in energy even though all three second-shell waters form two hydrogen bonds to the inner shell. This is because the pseudo-tetrahedral inner shell must distort severely to allow the third second-shell water to hydrogen bond to inner-shell waters already binding the other second-shell water ligands. The (5,2)_4D_2A_bA_b structure of the $n = 7$ complex has both second-shell waters doubly bound across from each other to the base of the square pyramid and is comparable in geometry to the complex reported by Hartmann et al.[15] Four other (5,2) isomers were located, 1−16 kJ/mol higher in energy (Table S1 and Figure S3f). No high-energy isomers for the (6,1)_AA structure were investigated in the present work, as Pavlov et al. reported a slight preference for the seventh water being doubly hydrogen bonded to the octahedral inner shell instead of a single hydrogen bond, with these two isomers being very close in energy (<1 kJ/mol).[18] A (7,0) complex was investigated here, but in agreement with the work of Hartmann et al.,[15] the (7,0) structure would always rearrange to the (6,1)_AA during optimization. Both of these previous studies neglected calculations of the (4,3) complexes.

In the $Zn^{2+}(H_2O)_8$ complex, for which previous theoretical results are not available, the tetrahedral 4-coordinate structure rises in energy at 0 K and the square pyramidal 5-coordinate inner shell is the lowest energy structure at all four levels of theory (Table 2). This transition results from both distortions in the tetrahedral inner shell that result as the eighth water is added (Table S2) and to the fact that the eighth water must be singly hydrogen bonded whereas the (5,3)_3AA and (6,2)_2D,DD_2AA structures allow the eighth water to form two hydrogen bonds (Figure 3) thereby lowering the energies of these structures. The (4,4)_2D,2DD_2AA,2A structure adds two singly hydrogen bonded water molecules to (4,2)_2AA. At 298 K, these two singly bound second-shell water ligands raise the entropy of this complex, such that this four-coordinate structure is lowest in free energy at the Bx levels. Another five (4,4) isomers are detailed in the Supporting Information. Three (5,3) isomers were located with the lowest energy 0 K structure, (5,3)_3AA, having all three second-shell waters doubly hydrogen bonded to the inner-shell waters, with two connected to opposite pairs of base inner-shell waters and the third connecting the apex water with a base water. This structure is also lowest in free energy at the Mx levels. The (6,2)_2D,DD_2AA and (6,2)_4D_2AA structures differ by less than 1 kJ/mol in energy (Table 2). Both have two second-shell waters doubly hydrogen bonded to the inner shell, but in the lower energy structure, one of the inner-shell waters is shared by the second-shell waters, whereas in (6,2)_4D_2AA, they use two different pairs of inner-shell waters (Figure 3). The former structure allows for the retention of more hydrogen-bonding interactions among the inner-shell waters. At 298 K, Bx calculations predict the six-coordinate complexes to be much higher in free energy (23−25 kJ/mol); however, Mx calculations predict both (6,2) complexes to be only 2−7 kJ/mol higher in free energy.

In $Zn^{2+}(H_2O)_9$, the tetrahedral 4-coordinate structure again rises in energy relative to the (5,4)_4A_bA_b, which is the ground-state geometry at all four levels of theory. The (6,3)_6D_3AA structure also lowers slightly in energy as the ninth water doubly hydrogen bonds to the inner shell forming a complex with D_3 symmetry (Figure S1). There are six isomers located with a 4-coordinate inner shell, as described in the Supporting Information. The lowest of these, (4,5)_D,3DD_2AA,3A, has two second-shell waters doubly hydrogen bonded with the other three waters all singly hydrogen bonded to inner-shell waters. There are also six isomers of the 5-coordinate complexes, with the lowest, (5,4)_4A_bA_b, having all 4 outer shell waters forming two hydrogen bonds to the base of the square pyramid inner shell. Although this (5,4) structure is lowest in enthalpy at 0 K, its 298 K free energy is 10 kJ/mol higher than the (4,5) at the Bx levels (6 and 15 kJ/mol lower at MP2 and M06, respectively). The (6,3)_6D_3AA maximizes the distance between the second solvent shell waters such that no inner-shell water is bound to two different second-shell waters. The (6,3)_4D,DD_3AA complex is ∼2−3 kJ/mol higher in energy than (6,3)_6D_3AA because one inner-shell water is shared between two second-shell waters. At 298 K, (6,4)_4D,DD_3AA becomes lower in free energy by about 2−3 kJ/mol because one inner-shell water is not constrained by a H bound to a second-shell water.

For the $Zn^{2+}(H_2O)_{10}$ complex, again the 5-coordinate inner-shell structure, (5,5)_4A_bA_b,A_a is lowest in energy and can be formed by adding the tenth water singly hydrogen bonded to the apex water of the symmetric (5,4)_4A_bA_b structure. However, the tetrahedral (4,6)_2AA,4A structure is relatively low in energy, has D_{2d} symmetry, and can be formed by singly hydrogen bonding four second-shell waters to the inner solvent shell of the (4,2)_2AA structure (Figure 1). In (6,4)_4D,2DD_4AA, which has C_2 symmetry, the second shell is orientated in such a way that two inner solvent shell water ligands must each share two different second-shell waters, i.e., the binding motif illustrated in the (6,2)_2D,DD_2AA complex (Figure 3).

Comparison to Calcium Water Clusters. In contrast to the ambiguity of the inner coordination shell of Zn^{2+}, our previous studies of Ca^{2+} hydration[41] indicate that the 6-coordinate inner shell is the clear ground-state configuration, being lower in energy by 10−23 kJ/mol compared to the 5-coordinate and lower by 24−47 kJ/mol compared to the 4-coordinate, depending on the level of theory for the $n = 6$ complexes. This assignment has now been confirmed by recent spectroscopic studies.[64] The 6-coordinate structures remain the ground states for larger $Ca^{2+}(H_2O)_n$ complexes (up to $n = 11$) with structures similar to the lowest energy structures found here. The (6,2)_2D,DD_2AA and (6,2)_4D_2AA isomers are similar to the two lowest energy structures discussed previously for $Ca^{2+}(H_2O)_8$, although there the (6,2)_4D_2AA structure is lower

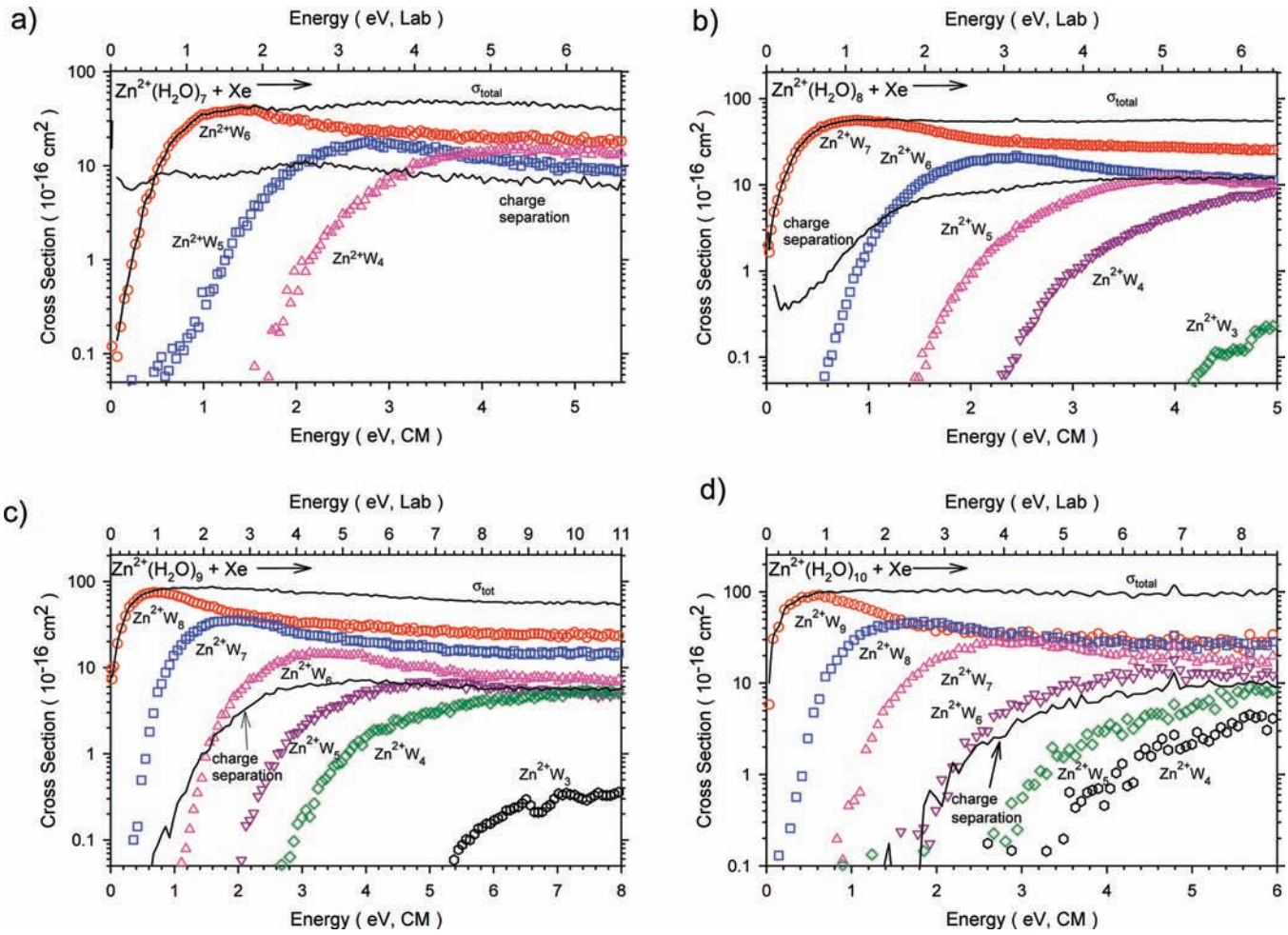

Figure 4. CID cross sections for the sequential water loss (open symbols) and charge separation processes (line) for $Zn^{2+}W_n$ where $n = 7-10$ and $W = H_2O$ (parts a−d, respectively) colliding with Xe at 0.2 mTorr as a function of energy in the laboratory (upper x-axis) and center of mass (lower x-axis) frames.

in energy by 2.2−2.6 kJ/mol. Also, the (6,3)_ 6D_3AA structure was found to be the ground-state structure of $Ca^{2+}(H_2O)_9$.

Interestingly, the calculated distances from the metal ion to the inner-shell oxygens are 0.2−0.4 Å larger for Ca^{2+} compared to Zn^{2+} for all complex sizes. This difference directly reflects the relative ionic radii of Ca^{2+} versus Zn^{2+}, 1.05 and 0.78 Å, respectively,[65] which can be attributed to the higher nuclear charge of Zn^{2+} with the additional 10 electrons added to the 3d core orbitals. Compared to Ca^{2+}, which has a rare gas electron configuration, the ambiguity of the most stable inner shell for zinc can be understood in part by the 18 e^- rule, which is satisfied by $Zn^{2+}(H_2O)_4$, lending this inner shell enhanced stability compared to those where more waters are directly bonded to the metal ion.

CID Cross Sections. Experimental cross sections for collision-induced dissociation with Xe were acquired for $Zn^{2+}(H_2O)_n$ where $n = 7-10$, as shown in Figure 4. In all cases, the dominant reactions are the loss of a single water molecule, reaction 1, followed by loss of additional water molecules as the translational energy increases. The smallest zinc water complex observed was $Zn^{2+}(H_2O)_3$ (Figure 4b,c) which has a cross section that is considerably smaller than that of the $Zn^{2+}(H_2O)_4$ product. In addition, the energy gap between the onsets of these two product ions is considerably larger than between any other pair of sequential products. These observations suggest that the $Zn^{2+}(H_2O)_4$ complex is particularly stable and may provide a clue as to the inner solvent shell of Zn^{2+}, as discussed further below. $ZnOH^+(H_2O)_n$ and $H^+(H_2O)_m$ products are also observed and shown as the total "charge separation" cross section in Figure 4a−d. These processes are discussed in detail in the following paper.[20] For the purposes of the present work, it is important to note that the $Zn^{2+}(H_2O)_7$ complex dissociates by charge separation in reaction 7 at lower energies than loss of a water molecule in reaction 1.

$$Zn^{2+}(H_2O)_7 + Xe \rightarrow ZnOH^+(H_2O)_3 + H^+(H_2O)_3 + Xe \quad (7)$$

Because the charge separation process 7 is energetically more favorable than the competing water loss reaction, competition between these channels shifts the apparent water loss threshold to higher energies. Including this competition for $n \leq 7$ is necessary when extracting accurate threshold energies, as discussed in detail in the following paper.[20]

Thermochemical Results. Cross sections for the primary and secondary dissociation products were analyzed using eqs 3 and 4 and the sequential dissociation model in several ways, with Table 3 summarizing the average modeling parameters used. Threshold E_0 values were determined for the primary dissociation of each complex from modeling with (eq 4) and without (eq 3) including RRKM theory. The difference between these results is the kinetic shift, which is appreciable for all complexes. The kinetic shifts for the water loss channels gradually increase

TABLE 3: Optimized Parameters of Eq 4 from Analysis of CID Cross Sections[a]

n	reactant	product	σ_0	N	kinetic shift (eV)	E_0 (PSL, eV)	$\Delta S^{\ddagger}_{1000K}$ (J/mol K)
10	(5,5)	(5,4)[b]	103 (3)	1.0 (0.1)	0.58 (0.04)	0.44 (0.03)	12 (4)
	(5,5)	(5,4)[c]	102 (4)	1.1 (0.1)	0.58 (0.07)	0.44 (0.06)	12 (4)
		(5,3)[c]	83 (5)	1.1 (0.1)		1.17 (0.03)	
	(5,5)	(5,4)[d]	103 (4)	1.0 (0.1)	0.58 (0.04)	0.44 (0.03)	12 (4)
		(6,3)[d,e]	103 (4)	1.0 (0.1)		0.48	10 (4)
	(5,5)	(5,4)[d]	103 (3)	1.0 (0.1)	0.58 (0.04)	0.44 (0.03)	12 (4)
		(4,5)[d,f]	103 (3)	1.0 (0.1)		0.50	80 (4)
	(5,5)	(4,5)[c]	101 (4)	1.1 (0.1)	0.55 (0.07)	0.47 (0.06)	79 (4)
		(5,3)[c]	84 (5)	1.1 (0.1)		1.14 (0.03)	
	(5,5)	(4,5)[c]	101 (4)	1.1 (0.1)	0.55 (0.07)	0.47 (0.06)	79 (4)
		(4,4)[c]	84 (5)	1.1 (0.1)		1.13 (0.03)	
	(4,6)	(5,4)[d]	103 (3)	1.0 (0.1)	0.64 (0.04)	0.38 (0.03)	−50 (4)
		(4,5)[d,f]	103 (3)	1.0 (0.1)		0.44	16 (4)
9	(5,4)	(5,3)[b]	92 (8)	0.9 (0.2)	0.42 (0.10)	0.55 (0.08)	54 (8)
	(5,4)	(5,3)[c]	92 (6)	0.9 (0.2)	0.40 (0.08)	0.57 (0.06)	57 (8)
		(4,3)[c]	58 (17)	0.9 (0.2)		1.31 (0.09)	
	(5,4)	(5,3)[c]	93 (6)	0.9 (0.2)	0.39 (0.08)	0.58 (0.06)	56 (8)
		(5,2)[c]	58 (17)	0.9 (0.2)		1.30 (0.09)	
	(5,4)	(5,3)[d]	92 (8)	0.9 (0.2)	0.42 (0.10)	0.55 (0.08)	54 (8)
		(6,2)[d,e]	92 (8)	0.9 (0.2)		0.62	75 (8)
	(5,4)	(5,3)[d]	92 (8)	0.9 (0.2)	0.42 (0.10)	0.55 (0.08)	54 (8)
		(4,4)[d,f]	92 (8)	0.9 (0.2)		0.57	90 (8)
	(4,5)	(5,3)[d]	91 (8)	0.9 (0.2)	0.50 (0.10)	0.47 (0.08)	−8 (8)
		(4,4)[d,f]	92 (8)	0.9 (0.2)		0.49	28 (8)
	(4,5)	(4,4)[b]	91 (8)	0.9 (0.2)	0.48 (0.10)	0.49 (0.08)	23 (8)
8	(5,3)	(4,3)[b]	67 (6)	0.8 (0.2)	0.34 (0.09)	0.71 (0.07)	65 (8)
	(5,3)	(4,3)[c]	68 (5)	0.8 (0.2)	0.33 (0.08)	0.72 (0.06)	67 (9)
		(4,2)[c]	48 (5)	0.8 (0.2)		1.68 (0.06)	
	(5,3)	(5,2)[d]	66 (6)	0.8 (0.2)	0.37 (0.09)	0.68 (0.07)	55 (8)
		(4,3)[d,e]	66 (6)	0.8 (0.2)		0.79	65 (8)
	(5,3)	(4,3)[d]	67 (6)	0.8 (0.2)	0.34 (0.09)	0.71 (0.07)	65 (8)
		(5,2)[d,f]	67 (6)	0.8 (0.2)		0.71	54 (8)
	(4,4)	(4,3)[d]	66 (6)	0.8 (0.2)	0.39 (0.09)	0.66 (0.07)	22 (8)
		(5,2)[d,f]	66 (6)	0.8 (0.2)		0.66	11 (8)
	(4,4)	(5,2)[b]	65 (6)	0.8 (0.2)	0.44 (0.09)	0.62 (0.07)	17 (8)
7	(4,3)	(4,2)[b]	58 (5)	0.7 (0.2)	0.20 (0.10)	0.89 (0.06)	18 (7)
	(4,3)	(4,2)[c]	58 (7)	0.8 (0.2)	0.21 (0.11)	0.88 (0.07)	19 (10)
		(4,1)[c]	37 (10)	0.8 (0.2)		2.02 (0.09)	
	(5,2)	(6,0)[c]	58 (7)	0.8 (0.2)	0.19 (0.11)	0.90 (0.07)	63 (10)
		(5,0)[c]	37 (10)	0.8 (0.2)		2.00 (0.09)	
	(5,2)	(5,1)[c]	58 (7)	0.8 (0.2)	0.14 (0.11)	0.95 (0.07)	76 (10)
		(5,0)[c]	37 (10)	0.8 (0.2)		1.98 (0.09)	
	(5,2)	(6,0)[d]	58 (5)	0.7 (0.2)	0.18 (0.10)	0.91 (0.06)	62 (7)
		(4,2)[d,e]	58 (5)	0.7 (0.2)		0.95	28 (7)
	(5,2)	(6,0)[d]	57 (5)	0.7 (0.2)	0.16 (0.10)	0.92 (0.06)	62 (7)
		(5,1)[d,e]	57 (5)	0.7 (0.2)		0.96	73 (7)
	(4,3)	(4,2)[d]	58 (5)	0.7 (0.2)	0.20 (0.10)	0.89 (0.06)	18 (7)
		(5,1)[d,f]	58 (5)	0.7 (0.2)		0.98	67 (7)
	(4,3)_[g]	(4,2)[d]	58 (5)	0.7 (0.2)	0.28 (0.10)	0.81 (0.06)	−29 (7)
		(5,1)[d,f]	58 (5)	0.7 (0.2)		0.90	18 (7)

[a] Uncertainties in parentheses. [b] Single channel modeling using eq 4. [c] Sequential dissociation modeling using eqs 4 and 6. [d] Composite modeling using eq 4. [e] Difference between the higher and lower energy threshold is given by MP2(full) results for respective complex sizes. [f] Difference between the higher and lower energy threshold is given by Bx results for respective complex sizes. [g] (4,3)_2D,DD_AA,2A isomer.

as the complex gets larger. Notably, cross sections could not be reproduced with fidelity in the threshold region when fitting the water loss channels with eq 3, whereas including RRKM theory in eq 4 allows the kinetic energy dependence of the cross sections to be modeled accurately over a wide range of energies.

One complication with the analyses conducted here is that the results depend on the isomers assumed for the reactants and products. It should be realized that these changes in the threshold values are not a result of experimental error, but of the ambiguity in the theoretical calculations regarding the GS structures of the reactant and product complexes. Because theory provides ambiguous guidance about which isomers are favored, the analyses summarized in Table 3 include all pertinent permutations of the predicted EMs and TSs, as discussed below for each complex.

***n* = 9 and 10.** For $Zn^{2+}(H_2O)_{10}$ and $Zn^{2+}(H_2O)_9$, there are no charge separation processes competing with either the primary or secondary water loss channels (Figure 4). For both complexes, the primary water loss dissociation is modeled simply by using eq 4 and the secondary water loss is modeled by introducing the secondary dissociation using eq 6. A representative model is shown in Figure 5a for the sequential dissociation of $Zn^{2+}(H_2O)_9$, assumed to have the (5,4)_4A_bA_b ground-state geometry, or (5,4) (from this point forward we abbreviate our naming scheme to (x,y) for the lowest energy isomer of each inner solvent shell). We find that the primary

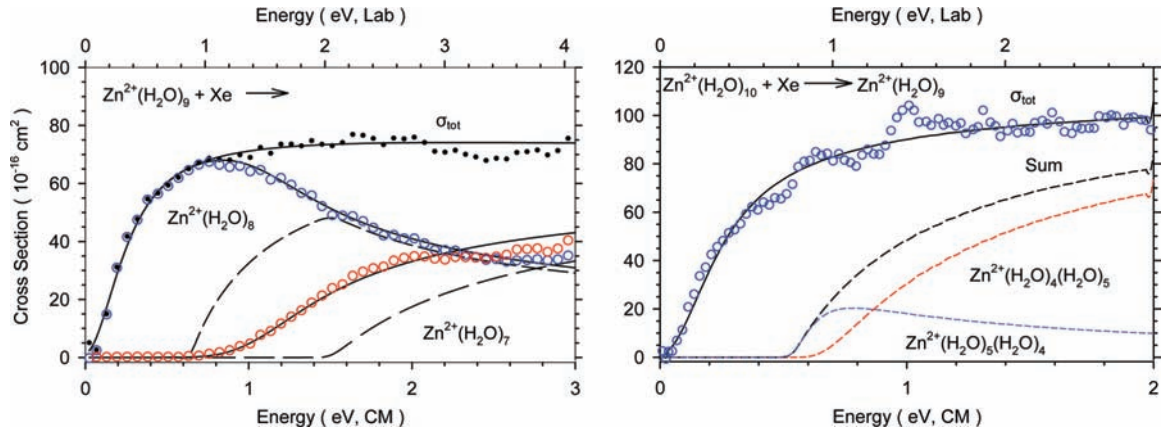

Figure 5. Zero pressure extrapolated cross sections for the CID of $Zn^{2+}(H_2O)_9$ (a, left) and $Zn^{2+}(H_2O)_{10}$ (b, right) with Xe. Solid lines show the best fits to both the primary and secondary water loss using eqs 4 and 6 convoluted over the kinetic and internal energy distributions of the neutral and ion. Dashed lines show the absence of experimental kinetic energy broadening for reactions with an internal energy of 0 K. In part b, the relative energy between the (5,4) and (4,5) products is set to the 0.06 eV value from Bx calculations. Optimized parameters for these fits are found in Table 3.

thresholds obtained are independent of whether the sequential dissociation channel is included in the modeling or not (Table 3). However, small differences are observed depending on the isomers assumed for the reactants and products. If the $Zn^{2+}(H_2O)_{10}$ data is analyzed using molecular parameters appropriate for the (5,5) isomer dissociating to (5,4) + H_2O, then the threshold is 0.44 ± 0.03 eV, whereas dissociation to (4,5) + H_2O yields a slightly higher threshold of 0.47 ± 0.06 eV, and a (4,6) → (5,4) + H_2O dissociation gives a lower threshold by 0.06 eV. Likewise, analysis of $Zn^{2+}(H_2O)_9$ data assuming a (4,5) reactant has a threshold that is 0.08 eV lower than the (5,4) reactant (Table 3). These changes in measured thresholds are the result of differing kinetic shifts in all cases. When the reactants have four inner-shell water ligands, there are more outer-shell waters with lower torsional frequencies, which leads to a higher density of states and a much lower entropy of activation (by 60 J/(mol K), Table 3) than when the reactants have a five water inner shell. Because of this restriction, the rates of dissociation decrease thereby increasing the kinetic shift and lowering the 0 K threshold for the four water inner-shell complexes. Overall, there is no experimental means of ascertaining which interpretation of the data is preferred, so multiple values are discussed below in comparison to theoretical bond energies.

In the analyses discussed above, it was assumed that a single reactant isomer dissociates to a single product isomer, whereas several product isomers could conceivably be formed from any reactant. To consider this, we analyzed the data assuming that a single EM could dissociate to multiple product channels, such that several dissociation channels (each leading to a product having the same mass) compete, as modeled using eq 4. In these "composite" models, the energy difference between product channels was fixed at the theoretical difference calculated at either the Bx (an average of B3LYP and B3P86) or MP2(full) levels. This method of analysis may better describe changes in the kinetic shift resulting from different entropies and densities of states of each product channel. A representative model is shown in Figure 5b for the composite fitting of (5,5) dissociating to both (5,4) + H_2O and (4,5) + H_2O using the Bx predicted relative energy of 0.06 eV between these two product channels. Dissociation to (5,4) is the lowest energy pathway; however, above about 0.85 eV, the (4,5) product dominates (Figure 5b), because it has a larger number of states resulting from the singly hydrogen bonded outer shell water ligand. Thus, the (5,5) → (4,5) + H_2O dissociation is faster according to RRKM rate theory and will have a smaller kinetic shift than the (5,5) → (5,4) + H_2O dissociation. Although the (4,5) product channel does not directly affect the threshold, it controls the high energy shape of the cross section, potentially influencing the N value in eq 4 used to reproduce the data, which could indirectly shift the measured threshold. In practice, we find that such composite fits of the data do not lead to significant shifts in the N values or measured thresholds (in all cases, changes in E_0 of less than 0.01 eV, Table 3). Thus, composite fits may very well be more accurate representations of the dissociation phenomena occurring but do not influence the thermochemistry derived.

In our analysis of the $Zn^{2+}(H_2O)_{10}$ data, the difference between the primary and secondary thresholds is 0.73 ± 0.03 eV when treated as (5,5) → (5,4) + H_2O → (5,3) + 2 H_2O, 0.67 ± 0.03 eV when treated as (5,5) → (4,5) + H_2O → (5,3) + 2 H_2O, and 0.66 ± 0.03 eV when treated as (5,5) → (4,5) + H_2O → (4,4) + 2 H_2O. Analysis of the $Zn^{2+}(H_2O)_9$ data yields a primary - secondary threshold difference of 0.74 ± 0.09 eV when treated as (5,4) → (5,3) + H_2O → (4,3) + 2 H_2O. These threshold energy differences are more precise than the differences in the absolute threshold energies listed in Table 3 because several systematic uncertainties cancel. The latter value of 0.74 ± 0.09 eV agrees well with that obtained from the 0.71 ± 0.07 eV threshold for the primary dissociation processes, reaction 1 modeled as (5,3) → (4,3) + H_2O. In contrast, the primary−secondary threshold difference for n = 10 of 0.73 ± 0.03 eV is higher in energy than the 0.55 ± 0.08 eV value given by the primary dissociation of n = 9, reaction 1 modeled as (5,4) → (5,3) + H_2O. Likewise, the 0.67 ± 0.03 and 0.66 ± 0.03 eV threshold differences are similarly higher than the primary threshold when modeled in a self-consistent manner, namely as (4,5) → (5,3) + H_2O and (4,5) → (4,4) + H_2O, respectively. This result is discussed further below.

***n* = 7 and 8.** Analysis of the primary reaction pathways of $Zn^{2+}(H_2O)_8$ and $Zn^{2+}(H_2O)_7$ considering various reactant and product isomers yields similar results as the n = 9 and 10 complexes. The (4,4) → (4,3) + H_2O dissociation yields an E_0 value that is 0.05 eV lower than the (5,3) → (4,3) + H_2O dissociation, which has a threshold of 0.71 ± 0.07 eV. As for the larger complexes, this increase is a result of the larger number of low torsional frequencies of the (4,4) compared to the (5,3) reactant, such that the entropy of activation decreases by 40 J/(mol K) (Table 3). We also find that a (5,3) → (5,2) +

TABLE 4: Comparison of Experimental 0 K Bond Energies (kJ/mol) to Theoretical Values[a]

n	reactant	product	expt	B3LYP//B3LYP[b]	B3P86//B3LYP[b]	M06//B3LYP[b]	MP2(full)//B3LYP[b]	MP2(FC)//RHF[c]	B3LYP//B3LYP[d]	B3LYP//B3LYP[e]	MP2//HF[f]
6	(4,2)	(4,1)	**98.4**[g,h] **(3.9)**	**97.0**	**100.6**	103.7	95.7		101.3	100.8[l]	95.0
			109.0[h] (4.8)								
	(6,0)	(5,0)	**94.6**[g,h]**(3.9)**	87.1	90.1	**110.2**	**93.6**	123.1[l]	91.2		110.9
			105.8[h] (4.8)								
7	(4,3)	(4,2)	78.2[g] (4.8)	79.8	82.5	78.3	76.5				
			92.6[h] (5.8)								
	(4,3)[j]	(4,2)	**71.4**[g] **(4.8)**	**75.7**	**78.4**	69.6	69.3				
	(5,2)	(6,0)	**79.2**[g] **(4.8)**	93.5	97.0	**81.7**	**83.3**				
	(6,1)	(6,0)		75.1					76.6		
	(5,2)	(4,2)		79.7						87.9	
8	(4,4)	(4,3)	**63.7**[g] **(5.8)**	**74.8**	**77.0**	76.4	72.7				
	(5,3)	(4,3)	70.4[g] (5.8)	**75.8**	**78.6**	96.3	86.3				
			71.4[h] **(8.7)**								
	(5,3)	(5,2)	**67.5**[g] **(5.8)**	76.0	78.8	**81.4**	**75.4**				
			69.5[h] **(8.7)**								
9	(4,5)	(5,3)	**45.3**[k] **(7.7)**	**65.6**	**66.8**	49.5	50.9				
			64.6[h] (2.9)								
	(5,4)	(5,3)	**53.1**[k] **(7.7)**	**70.8**	**72.5**	**79.4**	**71.6**				
			70.4[h] **(2.9)**								
10	(4,6)	(5,4)	**36.7**[k] **(2.9)**	**57.2**	**58.1**	34.3	40.2				
	(5,5)	(5,4)	**42.5**[k] **(2.9)**	60.6	62.4	**61.5**	**59.0**				

[a] Values in bold highlight the experimental threshold energies interpreted on the basis of the corresponding theoretical value. [b] Geometry optimizations calculated using a B3LYP/6-311+G(d,p) level and SPE values calculated with a 6-311+G(2d,2p) basis set for each level. ZPE and cp corrected. [c] Values reported by Bock et al. using MP2(FC)/HUZSP*//RHF/HUZSP*.[14] [d] Values reported by Pavlov et al. using B3LYP/6-311+G(2d,2p)//B3LYP/ LANL2DZ.[18] [e] Values reported by Hartmann et al.[15] using B3LYP/SHA1//B3LYP/SHA3. [f] Values reported by Lee et al.[16] using MP2/TZ2P//HF/TZ2P. [g] Values including competitive shift reported in following publication.[20] [h] Sequential dissociation modeled using eqs 4 and 6. [l] No counterpoise correction. [j] (4,3)_2D,DD_AA,2A isomer. [k] Single-channel model using eq 4.

H_2O pathway has a lower threshold than (5,3) → (4,3) + H_2O by 0.03 eV, because the former product is more constrained than the latter (with a change in the entropy of activation of only 10 J/K mol). Similarly, the (4,4) → (5,2) + H_2O dissociation has the lowest threshold and entropy of activation of 0.62 ± 0.07 eV and 17 ± 8 J/(mol K), respectively, because this dissociation involves the loosest reactant dissociating to the most constrained product.

More dissociation pathways were analyzed for the dissociation of $Zn^{2+}(H_2O)_7$ because theory predicts multiple low energy structures of the reactant and product. Comparing the (4,3) → (4,2) + H_2O dissociation, which has an E_0 value of 0.89 ± 0.06 eV, (5,2) → (6,0) + H_2O is only 0.01−0.03 eV higher in energy (depending on whether a composite analysis is used and what the higher energy channel is), well within experimental uncertainty. Lower in energy is the dissociation of (4,3)_2D,DD_AA,2A to the (4,2) complex having an E_0 value of 0.81 ± 0.06 eV, a difference of 0.08 eV. This shift is relatively large because two of the three second-shell waters are singly hydrogen bonded in (4,3)_2D,DD_AA,2A, whereas only one of them is in (4,3). This leads to a change in the entropy of activation of about 50 J/(mol K).

For sequential dissociation of $Zn^{2+}(H_2O)_8$, modeled as (5,3) → (4,3) + H_2O → (4,2) + $2H_2O$, the difference between the primary and secondary thresholds yield 0.96 ± 0.06 for the dissociation energy of $Zn^{2+}(H_2O)_6$−H_2O. This value agrees with the threshold value obtained from the primary dissociation process of $Zn^{2+}(H_2O)_7$ modeled as (4,3) → (4,2) + H_2O, 0.89 ± 0.06 eV. In this system, derivation of accurate thermochemistry requires that the modeling should take into account the competition between the water loss and charge separation processes using eq 4. This is described fully in the following paper.[20]

In our analysis of the sequential dissociation of $Zn^{2+}(H_2O)_7$, a number of reactant and product isomers were again considered. When modeled as (4,3) → (4,2) + H_2O → (4,1) + $2H_2O$, the difference between the primary and secondary thresholds is 1.13 ± 0.05 eV. When modeled as (5,2) → (6,0) + H_2O → (5,0) + $2H_2O$, the difference between the primary and secondary E_0 values is 1.10 ± 0.05 eV, within experimental uncertainty. However, the difference between the primary and secondary thresholds is 1.03 ± 0.05 eV, 0.10 eV lower in energy, when the data is analyzed assuming (5,2) → (5,1) + H_2O → (5,0) + $2H_2O$. Examination of Table 3 shows that this difference is a result of small changes in both the absolute primary (by 0.07 eV) and secondary (by 0.04 eV) thresholds. In both cases, the differences in the thresholds can be traced to changes in the kinetic shifts associated with the varying reactant and product isomers. For this secondary threshold, no primary threshold for the dissociation of $Zn^{2+}(H_2O)_6$ is available for the comparison as charge separation limits the size of the reactants to $n \geq 7$.

Experimental Bond Enthalpies: Primary and Secondary Values. Table 4 lists experimental 0 K hydration energies that are equated with the primary threshold energies and differences between the secondary and primary threshold energies, all taken from Table 3. Theoretical 0 K hydration energies calculated here at three levels of theory and from the literature are shown for comparison. The reactant and product isomers chosen for comparison in Table 4 are based on the relative 298 K free energies and 0 K enthalpies given in Table 2. For a primary threshold energy, the reactant isomer is assumed to be the 298 K GS (as this species should have the dominant population in a thermally equilibrated source) and the product isomer is the 0 K GS (as our threshold analysis is dominated by the lowest 0 K enthalpy species, Figure 5b). In contrast, the secondary thresholds correspond to the 0 K primary product GS isomer dissociating to the 0 K product GS isomer for each level of theory. Because Bx and Mx calculations give differing results for the various GS complexes, the data are interpreted using both the Bx and Mx GSs and then compared to the self-consistent theoretical value interpretation of the data. In Table 4, values in bold highlight the experimental threshold energy and its corresponding theoretical value.

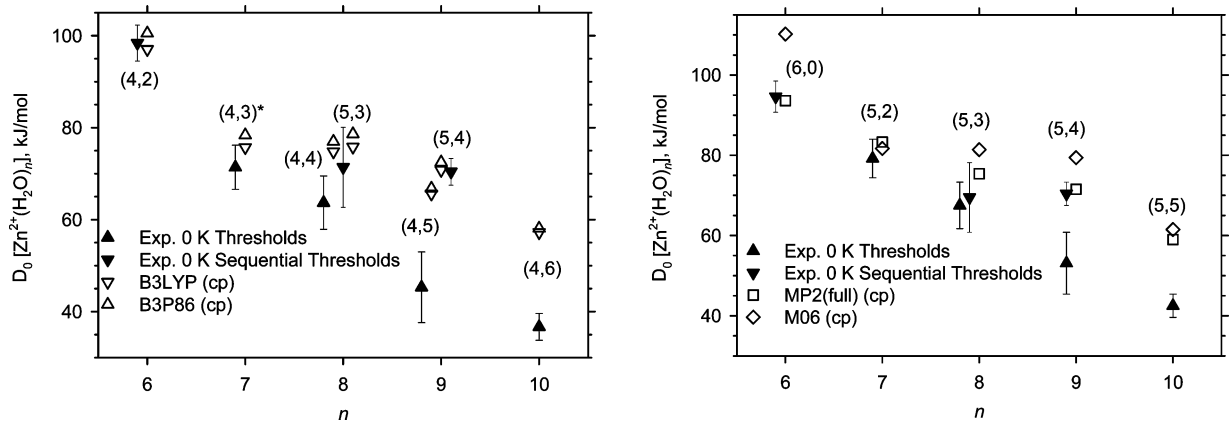

Figure 6. Comparison of experimental (solid symbols) and theoretical (open symbols) hydration enthalpies at 0 K for Bx (a, left) and Mx (b, right) results. All theoretical results shown are counterpoise corrected. The (4,3)* isomer corresponds to (4,3)_2D,DD_AA,2A.

For the $n = 6$ bond enthalpies, which can only be obtained from secondary thresholds for dissociation of $Zn^{2+}(H_2O)_7$ dissociating to $Zn^{2+}(H_2O)_5 + 2H_2O$, values were obtained including competition with the charge separation process, as accounted for and explained in the following paper,[20] and ignoring this competition. For both possible reactant isomers, (4,2) and (6,0), the value that includes this competition is lower, ranging from 94 to 99 kJ/mol, and is our best measurement of the $n = 6$ hydration energy. The energy difference between the values with and without competition is nearly constant, 10−11 kJ/mol for the two isomers, and is a measure of the competitive shift in this case.

Similar to the $n = 6$ complexes, the $n = 7$ complex exhibits a competitive shift of ~14 kJ/mol for the (4,3) → (4,2) + H_2O dissociation pathway (Table 4). (Although not explicitly examined, it is expected that similar shifts would occur for any of the other combinations of reactant/product isomers for the $n = 7$ complex, as was observed for the $n = 6$ system.) Note that the secondary threshold listed for $Zn^{2+}(H_2O)_8$ dissociating to $Zn^{2+}(H_2O)_6 + 2H_2O$, 0.96 ± 0.06 eV, agrees within experimental uncertainty with the primary dissociation threshold of $Zn^{2+}(H_2O)_7$ that does not account for competition, 0.89 ± 0.06 eV (Table 3). In both measurements, competition with charge separation has shifted the thresholds to higher energies. As for the $n = 6$ complex, our best experimental hydration energies for $n = 7$ are those obtained from the analyses that include competition, here the primary thresholds. These range from 71 to 79 kJ/mol (Table 4), depending on the various reactant and product isomers assumed in the analysis.

The water loss dissociation channel of the $n = 8$ complex is not affected significantly by competition with the charge separation channel that occurs at this complex size. Accordingly, the difference between 0 K hydration energies obtained from the primary and secondary dissociation channels are within 1−2 kJ/mol, well within experimental uncertainty. These values range from 63 to 72 kJ/mol (Table 4), depending on reactant and product isomers.

For the $n = 9$ complex, there is no charge separation channel competing with dehydration. We measure a difference between the primary and secondary E_0 values for the (5,5) → (5,4) + H_2O → (5,3) + $2H_2O$ process as 0.73 ± 0.03 eV, whereas the primary E_0 value for (5,4) → (5,3) + H_2O is lower, 0.55 ± 0.08 eV (Table 3). The difference between these two measurements (0.18 eV) is outside of experimental uncertainty (0.11 eV), and alternate isomer assumptions, (4,5) → (5,3) + H_2O, yield similar results (see above). One possible explanation for this difference hypothesizes that we are producing a distribution of isomers of these larger complexes in our ESI source. For instance, isomers of the $n = 8-10$ complexes having a 4-coordinate inner hydration shell are calculated to lie 15, 22, and 19 kJ/mol, respectively, above the 5-coordinate GSs at the MP2(full) level of theory (Table 2). According to the free energies of these species calculated at the MP2(full) level, a Boltzmann distribution at 298 K predicts the (4,5) structure to be 8% abundant. The presence of these higher energy isomers in our reactant ion beams could lead to primary dissociation thresholds that are low by amounts up to these excitation energies. However, using this example, if the $n = 9$ cross section is modeled assuming 92% (5,4) and 8% (4,5) isomers are present with an energy gap of 22 kJ/mol (0.23 eV) between them, the 0 K threshold determined changes by only 0.03−0.04 eV from analysis where only the (5,4) reactant is present. Notably, the relative Bx free energies of the (5,4) and (4,5) are reversed compared to the Mx energies, such that the (4,5) species would be calculated to comprise 98% of the reactant beam. In this case, virtually no change in threshold would occur if 2% excited isomers in the reactant ions were included in the analysis.

Unlike the primary dissociations, we do not believe that the difference between the primary and secondary dissociation thresholds is influenced by alternate isomers in the reactant beam. This is because even if the reactant ions have a distribution of isomers, the primary and secondary thresholds are lowered by the same amount of energy, such that the relative measurement is unaffected. It can also be noted that a distribution of primary product isomers, such as that shown in Figure 5b, will not influence the absolute secondary threshold because the thermodynamics cannot be dependent on the pathway used to produce the secondary product from reactant ions. From an experimental point of view, neither the primary threshold of 0.55 ± 0.08 eV nor the secondary threshold of 0.73 ± 0.03 eV can be discounted as a valid measurement for the (5,4) → (5,3) + H_2O process.

Comparison of Experimental and Theoretical Bond Energies. Parts a and b of Figure 6 are direct comparisons of experimental and theoretical 0 K hydration energies from Table 4. Figure 6a has experimental data interpreted using Bx predicted GS isomers compared to Bx theoretical hydration energies and Figure 6b compares the values obtained from Mx predicted isomers. As discussed above, there is no primary value for $n = 6$ as this complex cannot be formed in the ESI source because of the charge separation process, and there is no secondary value for $n = 7$ because competition with the charge separation process cannot be included in the analysis. Good agreement with theory is found for $n = 6$, for all reactant and product isomers,

but only when the effects of competition are included (Table 4), which verifies the importance of including the competitive shifts reported in the following paper.[20] This more sophisticated modeling is necessary to obtain accurate hydration energies for this complex size, yielding 98.4 ± 3.9 kJ/mol using the Bx predicted (4,2) isomer and 94.6 ± 3.9 kJ/mol for the Mx predicted (6,0) reactant. Both methods of data analysis give excellent agreement to their respective levels of theory with MADs (mean absolute deviations) between experiment and three of the four levels of theory: 1.8 kJ/mol for the Bx (4,2) isomer and 1.0 kJ/mol for the MP2(full) (6,0) reactant. In contrast, the M06 level predicts a binding energy for (6,0) that is 15.6 kJ/mol higher in energy than experiment and 16.6 kJ/mol higher than MP2(full). Overall, neither theory nor the precision of the data analysis allows an unambiguous determination of which isomer is the true ground state. Therefore, we show both individual dissociation pathways in Figure 6a and 6b.

Similar to the $n = 6$ dissociation, the experimental 0 K hydration energies for the different isomers of $n = 7$ vary between the (4,3)_2D,DD_AA,2A and (5,2) reactant species predicted by Bx and Mx, respectively. The (4,3)_2D,DD_AA,2A dissociation is lower by 8 kJ/mol, compared to the (5,2) dissociation, a difference that is attributed to a change in the kinetic shift as discussed above. The (4,3)_2D,DD_AA,2A dissociation gives reasonable agreement with Bx theory, MAD of 5.7 kJ/mol (Figure 6a). Threshold results interpreting the data using the (5,2) reactant also gives excellent agreement to Mx theory with a MAD of 3.3 kJ/mol (Figure 6b) within experimental uncertainty.

As for the $n = 7$ results, the 0 K hydration energies for the various isomers of $n = 8$ remain within experimental uncertainty of each other. Here more dissociation pathways are considered because the primary process is assumed as the lowest 298 K free energy reactant dissociating to the lowest 0 K product, but the secondary process is the lowest energy 0 K dissociation. In this case, Bx results predict a (4,4) → (4,3) + H_2O primary process and a (5,3) → (4,3) + H_2O secondary process with MADs of 12.2 and 5.8 kJ/mol, respectively. The Mx GS structure results are less ambiguous at the larger complex sizes, predicting the (5,3) → (5,2) + H_2O for both the primary and secondary processes (Figure 6b). The differences in these thresholds from MP2(full) theory are 7.9 and 5.9 kJ/mol, respectively, and increase to 13.9 and 11.9 kJ/mol for M06 theory, respectively. Overall, neither theory nor experiment are able to definitively ascertain which reactants or dissociations are truly active.

For the larger $n = 9$ and 10 water complexes, experimental E_0 values obtained using eq 4 assuming a five-water inner solvent shell for the reactants differ from theoretical results by 16−26 kJ/mol depending on the level of theory used to interpret the data. However, when the data is analyzed assuming a (5,5) → (5,4) + H_2O → (5,3) + $2H_2O$ dissociation pathway, predicted by both Bx and Mx, the relative secondary threshold obtained yields a binding energy for $n = 9$ that is in excellent agreement with theory, with a MAD of only 4.3 kJ/mol. This is in much better agreement with theory than the primary values. The primary value predicted by Bx is the (4,5) → (5,3) + H_2O dissociation, with a MAD of 20.9 kJ/mol (Figure 6a). The Mx levels again predict the primary process as the 5-coordinate dissociation. Although this is the same isomeric dissociation seen in the secondary value above, the primary process has a MAD of 22.5 kJ/mol lower than the energy predicted by theory (Figure 6b). Obviously the secondary value is in much better agreement with all three levels of theory. These deviations have several possible explanations. As discussed above, higher energy isomers could be present in the reactant ion beams, leading to primary dissociation thresholds that are lower than the calculated bond energies for the GSs. In particular for these larger complexes, it seems possible that rehydration of smaller complexes in the hexapole region of the source could place a water ligand in a more weakly bound outer solvent shell, e.g., (5,3,1). As shown in the accompanying paper,[20] there can be appreciable barriers to rearrangement of such outer shell water molecules moving to more stable inner-shell positions. Another possible explanation is that thermalization of these larger complexes is not as complete as the smaller, more strongly bound complexes. Indeed, analysis indicates that the primary threshold would agree with that derived from the secondary threshold if the $n = 9$ reactant had a temperature of 500 K. However, such an analysis also necessitates lowering the N value such that the model no longer reproduces the data nearly as well, thereby discounting this hypothesis. Furthermore, a temperature of 500 K seems extraordinarily high for a source that has previously shown to produce thermalized ions.[37,41−43] The third explanation is that theory is not accurately accounting for the partially filled second solvent shell seen in the 8−10 water complexes. Rudolph et al. believed that the second hydration shell around Zn^{2+} is filled at $n = 18$ with an inner shell of 6, and any smaller structure with a partially filled second shell yielded a calculated binding enthalpy that would account for only 62−69% of the experimentally found single ion hydration enthalpy.[5] However, the study by Rudolph et al. only performed calculations using HF and MP2 levels of theory (with a variety of smaller basis sets compared to those used here) on the $n = 1-6$ and 18 complexes. On the basis of the calculations performed here, an inner solvent shell of six is consistently higher in energy than inner solvent shells of five and four for complexes up to $n = 10$, with the exception of the Mx results for the (6,0) complex. Pavlov et al. also addressed the importance of a filled second solvent shell for accurate binding energies and inner-shell size prediction. They concluded that larger cluster sizes of at least $n > 12$ were necessary to represent the dilute solutions found in spectroscopy experiments.[18] The importance of the second hydration sphere in the calculation of both frequencies and SPEs is seen both in the literature and in the work presented here for $n \geq 8$. Investigations are ongoing as to whether an alternate basis set or theoretical approach will more accurately account for this partially filled second shell.

For the $n = 10$ complexes, the primary processes are again much lower in energy than theory. If the data are interpreted as a 4-coordinate reactant dissociating to a 5-coordinate product (as predicted by Bx), the threshold, 36.7 ± 2.9 kJ/mol, has a MAD from theory of 20.9 kJ/mol (Figure 6a). This value actually agrees within experimental uncertainty with values calculated at the Mx levels of theory, however, this level of theory strongly supports the 5-coordinate GSs, leading to internal inconsistency. Similarly, the (5,5) → (5,4) + H_2O process supported by Mx has a threshold of 42.5 ± 2.9 kJ/mol, with a MAD compared to theory of 17.8 kJ/mol (Figure 6b). If a temperature of 500 K for the reactant is used in the analysis, the threshold increases to 50.3 kJ/mol giving a MAD of 10.0 kJ/mol. However, raising the temperature of the reactant means that the model fails to reproduce the data well and gives a threshold for $n = 10$ that is still lower in energy than that predicted by theory. Because primary thresholds for both $n = 9$ and 10 are low compared to theory, and the secondary value for $n = 9$ agrees, we do not believe these primary thresholds represent our best experimental values.

TABLE 5: Conversion of 0 K Thresholds to 298 K Enthalpies and Free Energies for Water Loss from $Zn^{2+}(H_2O)_n$[a]

n	dissociation	ΔH_0[b]	$\Delta H_{298} - \Delta H_0$[c]	ΔH_{298}	$T\Delta S_{298}$[c]	ΔG_{298}
6	(4,2) → (4,1)	98.4 (3.9)	4.7 (0.4)	103.1 (3.9)	46.6 (1.0)	56.5 (4.1)
	(6,0) → (5,0)	94.6 (3.9)	2.1 (0.5)	96.7 (3.9)	45.5 (1.4)	51.2 (4.1)
7	(4,3)_[d]→ (4,2)	71.4 (4.8)	−1.0 (0.3)	70.4 (4.8)	17.9 (1.4)	52.5 (5.0)
	(5,2) → (6,0)	79.2 (4.8)	6.2 (0.3)	85.4 (4.8)	39.1 (1.2)	46.3 (4.9)
8	(4,4) → (4,3)	63.7 (5.8)	1.1 (0.3)	64.8 (5.8)	34.6 (1.6)	30.2 (6.0)
	(4,4) → (5,2)	59.8 (5.8)	1.6 (0.2)	61.4 (5.8)	29.8 (1.1)	31.6 (5.9)
	(5,3) → (4,3)	71.4 (5.8)	3.6 (0.6)	75.0 (5.8)	46.0 (1.2)	29.0 (5.9)
	(5,3) → (5,2)	67.5 (5.8)	4.2 (0.4)	71.7 (5.8)	41.2 (1.1)	30.5 (5.9)
9	(4,5) → (5,3)	45.3 (7.7)	−1.4 (0.1)	43.9 (7.7)	20.7 (1.6)	23.2 (7.9)
	(5,4) → (5,3)	53.1 (7.7)	2.6 (0.4)	55.7 (6.8)	40.6 (1.1)	15.1 (7.8)
10	(4,6) → (5,4)	36.7 (2.9)	−3.2 (0.04)	33.5 (2.9)	10.9 (1.4)	22.6 (3.2)
	(5,5) → (5,4)	42.5 (2.9)	1.1 (0.3)	43.6 (2.9)	29.2 (1.0)	14.4 (3.1)

[a] All values in kJ/mol with uncertainties in parentheses. [b] Experimental values from Table 4. [c] Values calculated from the vibrations and rotations calculated at the B3LYP/6-311+G(d,p) level. Uncertainties found by scaling the frequencies up and down by 10%. [d] (4,3)_2D,DD_AA,2A isomer.

Conversion from 0 to 298 K Thermodynamics. Using the vibrational frequencies and rotational constants of the zinc water clusters calculated at the B3LYP/6-311+G(d,p) level of theory discussed above, a rigid rotor/harmonic oscillator approximation was applied to convert the 0 K bond energies to 298 K hydration enthalpies (Table 5). The uncertainties in these conversions are found by scaling the vibrational frequencies up and down by 10%. This approximation may not be suitable for all cases because of the low frequency torsional motions. Nevertheless, values appropriate for the GS species as determined from single-point energies and free energies at both the Bx and Mx levels of theory were considered, as discussed above. When looking at the different reaction pathways in Table 5, it can be noted that changes in the $T\Delta S_{298}$ values are inversely related to changes in the kinetic shift from Table 3. As the kinetic shift increases, the hydration energy decreases and both the entropy of activation and dissociation also decrease.

Comparing the dissociation pathways selected for Figure 6a (those predicted by Bx), the free energy values (ΔG_{298}) decrease as the complex gets larger. For the predicted primary dissociation pathways, the relative entropies of dissociation, $T\Delta S_{298}$, change as (4,2) > (4,3)_2D,DD_AA,2A < (4,4) > (4,5) > (4,6), whereas the secondary dissociations vary as (4,2) > (4,3) < (5,3) > (5,4) > (5,5). In general, the $T\Delta S_{298}$ value will increase as the relative number of states of the products increases or the number of states of the reactant decreases. Because the $T\Delta S_{298}$ values are calculated as the difference in the entropies of the product GS + H_2O and reactant GS, variations in the entropies of dissociation are largely dependent on the vibrational frequencies. If the reactant has more loose torsional frequencies compared to the product, the entropy of dissociation decreases. An example of this is seen in the large decrease (28.7 kJ/mol) from the (4,2) to (4,3)_2D,DD_AA,2A dissociations. Here the (4,3)_2D,DD_AA,2A has two single acceptor waters, "A", in the second solvent shell and thereby has more low torsional frequencies than the (4,2) complex where both second-shell waters form "AA" H-bonds. Overall, the patterns in dissociation entropies parallel those for the entropy of activation (discussed above for $n = 7-10$). Although the entropy of activation values are evaluated at 1000 K and do depend on details of the RRKM analysis, the variation in their values is also largely dependent on the changes in the vibrational frequencies of the EM and TS associated with solvent shell rearrangements.

Now looking at the dissociations predicted by the Mx levels of theory found in Figure 6b, the trend in $T\Delta S_{298}$ values can be explained using similar reasoning as that applied to the Bx predicted dissociations. Because the inner solvent shell remains constant at five waters, the relative entropies of dissociation remain fairly constant with values varying as (6,0) > (5,2) ~ (5,3) ~ (5,4) > (5,5). There is only a small decrease in the $T\Delta S_{298}$ from the (6,0) to (5,2) reactants. The latter complex undergoes an inner solvent shell rearrangement upon dissociation, which can have a more drastic affect on the $T\Delta S_{298}$ value, as seen above. However, both the (5,2) and (6,0) complexes have all water ligands bound relatively tightly with no singly hydrogen bound waters in the second shell, unlike the (4,3)_2D,DD_AA,2A complex.

Obviously, the $\Delta S^{\dagger}$, $T\Delta S_{298}$, and $\Delta\Delta G_{298}$ values (difference between the ΔG_{298} values of $Zn^{2+}(H_2O)_n$ and $Zn^{2+}(H_2O)_{n-1}$) of the water loss products are directly dependent on the GS structure chosen and will vary based on the inner solvent shell size and second-shell bonding. This emphasizes the need for careful analysis of all reaction dissociation pathways because of the ambiguous results of the theoretical calculations, especially in the cases where alternate isomers lead to changes in the kinetic shift large enough to alter the hydration energy. In addition to the dissociations chosen here for analysis in Table 4, all pathways analyzed in Table 3 are compared to theory and converted to 298 K in Tables S3 and S4 in the Supporting Information.

Conclusion

The energy-dependent cross sections of the collision-induced dissociation of $Zn^{2+}(H_2O)_7$, $Zn^{2+}(H_2O)_8$, $Zn^{2+}(H_2O)_9$, and $Zn^{2+}(H_2O)_{10}$ are determined using guided ion beam mass spectrometry. Experimental and theoretical bond dissociation energies for the $Zn^{2+}(H_2O)_n$ ($n = 6-10$) show a steady increase in energy as each water is removed agreeing with an intuitive understanding of metal ion hydration. Although the ESI source is limited to producing complexes of $n \geq 7$, our sequential dissociation model is able to provide additional thermochemical information for $n = 6$. Work is also underway to extend the sequential model to provide threshold analysis down to $Zn^{2+}(H_2O)_3$ which is the smallest zinc water cluster seen in the CID cross sections. Also, work has been performed analyzing the affect of the competition of the charge separation on the water loss thresholds, specifically those for the $n = 7$ and 6 binding energies. These results are discussed in detail in a separate publication on these processes.[20]

An exhaustive and thorough search into the low-energy structures of $Zn^{2+}(H_2O)_n$, where $n = 1-10$, is reported and examines inner-shell sizes of 4, 5, and 6. We find B3LYP and B3P86 calculations predict a GS with an inner shell of 4 up to

$n = 8$ where the GS switches to an inner shell of 5. This transition to a larger inner shell is a result of distortions in the tetrahedral inner shell and the need to bind outer-shell water ligands to the inner shell via single hydrogen bonds, both of which raise the energy of the 4-coordinate structure relative to the 5-coordinate. The average of the MADs between experiment and Bx theory reported in Figure 6a is 9.8 kJ/mol. In contrast, M06 and MP2(full) calculations show a preference of an inner shell of 5 for $n = 5$ and 7−10, and of 6 for $n = 6$. The average of the MADs between experiment and Mx theory in Figure 6b is 11.0 kJ/mol. This larger MAD is primarily because the M06 calculations generally overestimate the binding enthalpies, whereas the MAD between experiment and MP2(full) theory is 8.0 kJ/mol. Thus, it appears that MP2(full) gives the best agreement between experiment and theory for the water loss dissociation energies. For most values of *n*, both DFT and MP2 calculations show that all three inner-shell sizes are close in energy and a distribution of all isomers is experimentally possible. Because of this ambiguity, analysis of all dissociation pathways of the varying structures predicted by both levels of theory is carefully considered. Changes in the structures of the EM and TS lead to changes in the kinetic shift of the dissociation. Scrutiny of Figures 6a and 6b shows that Bx and MP2(full) theory provide similar agreement with experiment for the $n = 6$ and 7 complexes, but the Bx theoretical predictions of (4,4) and (4,5) GSs for $n = 8$ and 9 are inconsistent with the data. In contrast, the MP2 predictions of (5,3) and (5,4) GSs are in good agreement with our experimental results for $n = 8$ and 9. Although not definitive at this point, these comparisons suggest that the structural predictions of MP2 theory are more reliable. This means that most zinc complexes studied here have a five-coordinate inner hydration shell, with the exception being $Zn^{2+}(H_2O)_6$ where all ligands are bonded directly to the metal ion. Future work will look into the isomer distributions produced via ESI as well as theoretical calculations for the $n \geq 8$ complexes, which may better describe the binding energies of second solvent shell waters. Spectroscopic investigation of these complexes is also underway.

Acknowledgment. This work is supported by the National Science Foundation, Grant No. CHE-0748790. In addition, we thank the Center for High Performance Computing at the University of Utah for the generous allocation of computer time.

Supporting Information Available: Tables S1 and S2 provide relative energies and critical bond angles and lengths, respectively, of all $Zn^{2+}(H_2O)_n$ ($n = 6-10$) complexes. Table S3 provides the experimental and theoretical 0 K bond energies for all reactant and product isomers analyzed in Table 3. Table S4 is a conversion of the 0 K thresholds in Table S3 to 298 K enthalpies and free energies. Figures S1 and S2 show the low-lying isomers of $Zn^{2+}(H_2O)_9$ and $Zn^{2+}(H_2O)_{10}$. Figure S3 shows geometries for alternate isomers of all complexes. This material is available free of charge via the Internet at http://pubs.acs.org.

References and Notes

(1) Spiro, T. G. *Zinc enzymes*; J. Wiley: New York, 1983.
(2) Kimura, E. *Pure Appl. Chem.* **1993**, *65*, 355.
(3) Richens, D. T. *The Chemistry of Aqua Ions*; John Wiley and Sons, Inc: New York, 1997.
(4) Nriagu, J. O. *Zinc in the Environment*; Wiley: New York, 1980.
(5) Rudolph, W. W.; Pye, C. C. *Phys. Chem. Chem. Phys.* **1999**, *1*, 4583.
(6) Peschke, M.; Blades, A. T.; Kebarle, P. *Int. J. Mass Spectrom.* **1999**, *187*, 685.
(7) Peschke, M.; Blades, A. T.; Kebarle, P. *J. Am. Chem. Soc.* **2000**, *122*, 1492.
(8) Peschke, M.; Blades, A. T.; Kebarle, P. *J. Am. Chem. Soc.* **2000**, *122*, 10440.
(9) Shvartsburg, A. A.; Siu, K. W. M. *J. Am. Chem. Soc.* **2001**, *123*, 10071.
(10) Blades, A. T.; Jayaweera, P.; Ikonomou, M. G.; Kebarle, P. *Int. J. Mass Spectrom. Ion Processes* **1990**, *102*, 251.
(11) Chillemi, G.; D'Angelo, P.; Pavel, N. V.; Sanna, N.; Barone, V. *J. Am. Chem. Soc.* **2002**, *124*, 1968.
(12) D'Angelo, P.; Barone, V.; Chillemi, G.; Sanna, N.; Meyer-Klaucke, W.; Pavel, N. V. *J. Am. Chem. Soc.* **2002**, *124*, 1958.
(13) Pappalardo, R. R.; Marcos, E. S. *J. Phys. Chem.* **1993**, *97*, 4500.
(14) Bock, C. W.; Katz, A. K.; Glusker, J. P. *J. Am. Chem. Soc.* **1994**, *117*, 3754.
(15) Hartmann, M.; Clark, T.; vanEldik, R. *J. Mol. Model.* **1996**, *2*, 354.
(16) Lee, S.; Kim, J.; Park, J. K.; Kim, K. S. *J. Phys. Chem.* **1996**, *100*, 14329.
(17) Hartmann, M.; Clark, T.; vanEldik, R. *J. Am. Chem. Soc.* **1997**, *119*, 7843.
(18) Pavlov, M.; Siegbahn, P. E. M.; Sandstrom, M. *J. Phys. Chem. A* **1998**, *102*, 219.
(19) Wakita, H.; Johansson, G.; Sandstrom, M.; Goggin, P. L.; Hitotshi, O. J. *J. Sol. Chem.* **1991**, *20*, 642.
(20) Cooper, T.; Armentrout, P. B. *J. Phys. Chem. A*, DOI: 10.1021/jp906241q.
(21) Moision, R. M.; Armentrout, P. B. *J. Phys. Chem. A* **2006**, *110*, 3933.
(22) Roothan, C. C. J. *Rev. Mod. Phys.* **1954**, *23*, 69.
(23) Binkley, J. S.; Pople, J. A.; Hehre, W. J. *J. Am. Chem. Soc.* **1951**, *102*, 939.
(24) Frisch, M. J.; Trucks, G. W.; Schlegel, H. B.; Scuseria, G. E.; Robb, M. A.; Cheeseman, J. R.; Montgomery, Jr., J. A.; Vreven, T.; Kudin, K. N.; Burant, J. C.; Millam, J. M.; Iyengar, S. S.; Tomasi, J.; Barone, V.; Mennucci, B.; Cossi, M.; Scalmani, G.; Rega, N.; Petersson, G. A.; Nakatsuji, H.; Hada, M.; Ehara, M.; Toyota, K.; Fukuda, R.; Hasegawa, J.; Ishida, M.; Nakajima, T.; Honda, Y.; Kitao, O.; Nakai, H.; Klene, M.; Li, X.; Knox, J. E.; Hratchian, H. P.; Cross, J. B.; Bakken, V.; Adamo, C.; Jaramillo, J.; Gomperts, R.; Stratmann, R. E.; Yazyev, O.; Austin, A. J.; Cammi, R.; Pomelli, C.; Ochterski, J. W.; Ayala, P. Y.; Morokuma, K.; Voth, G. A.; Salvador, P.; Dannenberg, J. J.; Zakrzewski, V. G.; Dapprich, S.; Daniels, A. D.; Strain, M. C.; Farkas, O.; Malick, D. K.; Rabuck, A. D.; Raghavachari, K.; Foresman, J. B.; Ortiz, J. V.; Cui, Q.; Baboul, A. G.; Clifford, S.; Cioslowski, J.; Stefanov, B. B.; Liu, G.; Liashenko, A.; Piskorz, P.; Komaromi, I.; Martin, R. L.; Fox, D. J.; Keith, T.; Al-Laham, M. A.; Peng, C. Y.; Nanayakkara, A.; Challacombe, M.; Gill, P. M. W.; Johnson, B.; Chen, W.; Wong, M. W.; Gonzalez, C.; Pople, J. A. *Gaussian 03, revision B.02*; Gaussian, Inc.: Pittsburgh, PA, 2003.
(25) Becke, A. D. *J. Chem. Phys.* **1993**, *98*, 5648.
(26) Lee, C.; Yang, W.; Parr, R. G. *Phys. Rev. B* **1988**, *37*, 785.
(27) Ditchfield, R.; Hehre, W. J.; Pople, J. A. *J. Chem. Phys.* **1971**, *72*, 5639.
(28) Bauschlicher, C. W., Jr.; Partridge, H. *J. Chem. Phys.* **1995**, *103*, 1788.
(29) Perdew, J. P. *Phys. Rev. B* **1986**, *33*, 1788.
(30) Moller, C.; Plesset, M. S. *Phys. Rev. B* **1934**, *46*, 618.
(31) Zhao, Y.; Truhlar, D. G. *Theor. Chem. Acc.* **2008**, *120*, 215.
(32) Zhao, Y.; Truhlar, D. G. *Acc. Chem. Res.* **2008**, *41*, 157.
(33) Boys, S. F.; Bernardi, R. *Mol. Phys.* **1970**, *19*, 553.
(34) van Duijneveldt, F. B.; van Duijneveldt, J. G. C.; van Lenthe, J. H. *Chem. Rev.* **1994**, *94*, 1873.
(35) Becke, A. D. *J. Chem. Phys.* **1993**, *98*, 1372.
(36) Yu, W.; Liang, L.; Lin, Z.; Ling, S.; Haranczyk, M.; Gutowski, M. *J. Comput. Chem.* **2008**, *30*, 589.
(37) Moision, R. M.; Armentrout, P. B. *J. Am. Soc. Mass Spectrom.* **2007**, *18*, 1124.
(38) Kim, T.; Udseth, H. R.; Smith, R. D. *Anal. Chem.* **2000**, *72*, 5014.
(39) Shaffer, S. A.; Prior, D. C.; Anderson, G. A.; Udseth, H. R.; Smith, R. D. *Anal. Chem.* **1998**, *70*, 4111.
(40) Shaffer, S. A.; Tolmachev, A.; Prior, D. C.; Anderson, G. A.; Udseth, H. R.; Smith, R. D. *Anal. Chem.* **1999**, *71*, 2957.
(41) Carl, D. R.; Moision, R. M.; Armentrout, P. B. *Int. J. Mass Spectrom.* **2007**, *265*, 308.
(42) Heaton, A. L.; Ye, S. J.; Armentrout, P. B. *J. Phys. Chem. A* **2008**, *112*, 3328.
(43) Heaton, A. L.; Moision, R. M.; Armentrout, P. B. *J. Phys. Chem. A* **2008**, *112*, 3319.
(44) Carl, D. R.; Moision, R. M.; Armentrout, P. B. *J. Am. Soc. Mass Spectrom.* **2009**, in press.
(45) Ervin, K. M.; Armentrout, P. B. *J. Chem. Phys.* **1985**, *83*, 166.
(46) Muntean, F.; Armentrout, P. B. *J. Chem. Phys.* **2001**, *115*, 1213.
(47) Gerlich, D. *Adv. Chem. Phys.* **1992**, *82*, 1.
(48) Dalleska, N. F.; Honma, K.; Sunderlin, L. S.; Armentrout, P. B. *J. Am. Chem. Soc.* **1994**, *116*, 3519.
(49) Aristov, N.; Armentrout, P. B. *J. Phys. Chem.* **1986**, *70*, 4111.

(50) Daly, N. R. *Rev. Sci. Instrum.* **1960**, *31*, 264.
(51) Hales, D. A.; Lian, L.; Armentrout, P. B. *Int. J. Mass Spectrom. Ion Processes* **1990**, *102*, 269.
(52) Schultz, R. H.; Crellin, K. C.; Armentrout, P. B. *J. Am. Chem. Soc.* **1991**, *113*, 8590.
(53) Stein, S. E.; Rabinovich, B. S. *Chem. Phys. Lett.* **1977**, *49*, 1883.
(54) Beyer, T. S.; Swinehart, D. F. *Comm. Assoc. Comput. Mach.* **1973**, *16*, 379.
(55) Stein, S. E.; Rabinovich, B. S. *J. Chem. Phys.* **1973**, *58*−2438.
(56) Gilbert, R. G.; Smith, S. C. *Theory of Unimolecular and Recombination Reactions*; Blackwell Scientific: Oxford, UK, 1990.
(57) Holbrook, K. A.; Pilling, M. J.; Robertson, S. H. *Unimolecular Reactions*; Wiley: New York, 1996.
(58) Loh, S. K.; Hales, D. A.; Lian, L.; Armentrout, P. B. *J. Chem. Phys.* **1989**, *90*, 5466.
(59) Khan, F. A.; Clemmer, D. E.; Schultz, R. H.; Armentrout, P. B. *J. Phys. Chem.* **1993**, *97*, 7979.
(60) Rodgers, M. T.; Ervin, K. M.; Armentrout, P. B. *J. Chem. Phys.* **1997**, *106*, 4499.
(61) Rodgers, M. T.; Armentrout, P. B. *J. Chem. Phys.* **1998**, *109*, 1787.
(62) Armentrout, P. B.; Simons, J. *J. Am. Chem. Soc.* **1992**, *114*, 8627.
(63) Armentrout, P. B. *J. Chem. Phys.* **2007**, *126*, 234302.
(64) Bush, M. F.; Saykally, R. J.; Williams, E. R. *ChemPhysChem* **2007**, *8*, 2245.
(65) Wilson, R. G.; Brewer, G. R. *Ion Beams with Applications to Ion Implantation*; Wiley: New York, 1973.

JP906235Y